Title
Spatial control of Draper receptor signaling initiates apoptotic cell engulfment

Journal
Journal of Cell Biology, 217(11)

ISSN
0021-9525

Authors
Williamson, Adam P
Vale, Ronald D

Publication Date
2018-11-05

DOI
10.1083/jcb.201711175

Peer reviewed

JCB Journal of Cell Biology

ARTICLE

Spatial control of Draper receptor signaling initiates apoptotic cell engulfment

Adam P. Williamson[1,2] and Ronald D. Vale[1,2]

The engulfment of apoptotic cells is essential for tissue homeostasis and recovering from damage. Engulfment is mediated by receptors that recognize ligands exposed on apoptotic cells such as phosphatidylserine (PS). In this study, we convert *Drosophila melanogaster* S2 cells into proficient phagocytes by transfecting the Draper engulfment receptor and replacing apoptotic cells with PS-coated beads. Similar to the T cell receptor (TCR), PS-ligated Draper forms dynamic microclusters that recruit cytosolic effector proteins and exclude a bulky transmembrane phosphatase, consistent with a kinetic segregation-based triggering mechanism. However, in contrast with the TCR, localized signaling at Draper microclusters results in time-dependent depletion of actin filaments, which facilitates engulfment. The Draper–PS extracellular module can be replaced with FRB and FKBP, respectively, resulting in a rapamycin-inducible engulfment system that can be programmed toward defined targets. Collectively, our results reveal mechanistic similarities and differences between the receptors involved in apoptotic corpse clearance and mammalian immunity and demonstrate that engulfment can be reprogrammed toward nonnative targets.

Introduction

The prompt clearance of dying cells and debris is essential for maintaining homeostasis and promoting tissue repair (Reddien and Horvitz, 2004; Arandjelovic and Ravichandran, 2015; Neumann et al., 2015). In healthy tissue, resident and infiltrating phagocytes clear cell corpses and debris through specific recognition, uptake, and digestion (Elliott and Ravichandran, 2010). Defects in clearance result in autoimmunity and further tissue damage (Elliott and Ravichandran, 2010; Iram et al., 2016; Kawano and Nagata, 2018). Despite the importance of efficient clearance across multicellular life, mechanisms of engulfment receptor activation remain poorly understood in comparison with other signaling systems. Defining the molecular basis of engulfment receptor activation could lead to new strategies for enhancing clearance under conditions of extreme injury or programming phagocytes to eliminate functionally relevant targets such as cancer cells or pathogens.

The initial event in apoptotic cell clearance involves interactions of "eat-me" ligands exposed on dying cells with receptors on the phagocyte. Phosphatidylserine (PS) exposed on the outer leaflet of the plasma membrane constitutes one such eat-me ligand, although several other protein ligands likely participate as well (Fadok et al., 1992; Ravichandran and Lorenz, 2007; Segawa and Nagata, 2015). Ligand binding causes receptor phosphorylation, a process known as receptor triggering, and this event leads to cytosolic signaling that ultimately promotes cytoskeletal rearrangements that power corpse internalization (Reddien and Horvitz, 2004; Ravichandran and Lorenz, 2007). For most transmembrane receptors, triggering proceeds via one of two mechanisms: (1) ligand-induced receptor conformational change to transmit the signal across plasma membranes or (2) kinetic segregation, in which spatially organized zones of ligated receptors physically exclude phosphatases to favor net receptor phosphorylation and activation. EGF receptor and G protein–coupled receptors are examples of conformation-induced activation (Dawson et al., 2005; Erlandson et al., 2018), while the mammalian immune receptors that promote T cell activation and Fc receptor (FcR)–dependent engulfment of opsonized targets are triggered via a kinetic segregation mechanism (Davis and van der Merwe, 2006; Freeman et al., 2016). It remains unclear which activation mechanism corpse clearance receptors use to transmit the eat-me signal across phagocyte plasma membranes. In this study, we use receptor triggering as an inlet to address two open questions about engulfment signaling initiation: Do apoptotic ligands transmit a signal across the plasma membrane via a receptor conformational change or a kinetic segregation mechanism? How are ligated receptors

[1]Department of Cellular and Molecular Pharmacology, University of California, San Francisco, San Francisco, CA; [2]Howard Hughes Medical Institute, University of California, San Francisco, San Francisco, CA.

Correspondence to Ronald D. Vale: ron.vale@ucsf.edu.

organized on phagocyte plasma membranes to potentiate engulfment signaling?

To gain insight into these questions, we focused on Draper, a *Drosophila melanogaster* engulfment receptor. Draper is expressed in glia, where it promotes clearance of damaged axons, and in the somatic epithelium, where it functions to remove dying cells from the follicle (Freeman et al., 2003; MacDonald et al., 2006; Etchegaray et al., 2012). Draper is similar in domain structure to the mammalian protein Megf10 and to CED-1, the first described apoptotic corpse receptor in *Caenorhabditis elegans*. All three receptors contain single-pass transmembrane domains that connect extracellular EGF repeats to intracellular tyrosine (Tyr) phosphorylation sites that are presumed to recruit one or more downstream effectors (Zhou et al., 2001; Ziegenfuss et al., 2008; Scheib et al., 2012). Draper function has been dissected genetically, especially in its damaged axon clearance role, which defined a "parts list" of other proteins involved in engulfment signaling including Draper's cognate Src family kinase Src42a, the SH2-domain–containing kinase Shark, and the adapter protein Crk (Ziegenfuss et al., 2008, 2012; Lu et al., 2014). However, the mechanism by which receptor ligation leads to effector recruitment remains poorly understood.

In this study, we have reconstituted Draper-dependent engulfment in *Drosophila* S2 cells to dissect receptor triggering. We find that the lipid PS incorporated into lipid bilayers on beads is sufficient to induce receptor phosphorylation and a signaling cascade leading to engulfment. This system allows a dramatic reduction in the complexity of the apoptotic cell as the engulfment target. Similar to the T cell receptor (TCR), ligated Draper forms mobile microclusters that shift a kinase–phosphatase balance toward receptor phosphorylation. However, unlike TCR microclusters, Draper microclusters locally deplete F-actin. By mass spectrometry, we further demonstrate that phosphorylation of Draper is ordered and full activation of Draper requires an initial immunoreceptor Tyr-based activation motif (ITAM) phosphorylation followed by the modification of other Tyrs in its tail domain. We also reveal that the extracellular module of Draper and PS can be replaced with an artificial receptor and ligand that have an inducible interaction, providing another strategy for developing chimeric antigen receptors for phagocytosis (Morrissey et al., 2018). Our reconstitution of the initial steps of Draper signaling provides new insight into the mechanism of engulfment receptor triggering and a strategy to reprogram engulfment to new targets.

Results

Cellular reconstitution of Draper-dependent engulfment

We used cultured *Drosophila* S2 cells, which are derived from a hemocyte lineage (Schneider, 1972), as a cellular system for reconstituting corpse clearance. *Drosophila* S2 cells display a low level of engulfment of cell corpses (Fig. 1 A). We hypothesized that the level of engulfment might be low because S2 cells lack sufficient levels of engulfment receptors. For example, Draper is expressed at low levels in S2 cells as measured by RNA sequencing (Cherbas et al., 2011). To test whether introducing an exogenous engulfment receptor was sufficient to promote engulfment, we transfected S2 cells with Draper and assayed internalization of cell corpses using microscopy. Draper transfection increased the uptake of apoptotic cell corpses by approximately fivefold (Fig. 1 A). The overexpressed Draper-GFP and the endogenous Draper, which is expressed at approximately fivefold lower levels, show similar subcellular localization (Fig. S1 A).

The synapse between Draper-transfected S2 cells and corpses also served as a site of local receptor activation. After engaging with a damaged axon, Draper expressed in glial cells becomes Tyr phosphorylated at an ITAM motif, which then enables it to recruit a Syk-related Tyr kinase called Shark (Ziegenfuss et al., 2008). Consistent with the studies of Ziegenfuss et al. (2008), we find a specific recruitment of Shark-mCherry to the plasma membrane to the interface between the corpse and S2 cell (Fig. 1 B). Therefore, ligation of Draper to one or more ligands on a cell corpse is sufficient to trigger the local recruitment of the cytosolic tandem SH2-domain–containing kinase Shark and induce engulfment.

Apoptotic cells express an array of eat-me ligands (Ravichandran and Lorenz, 2007). As a next step, we sought to provide a homogenous synthetic target of uniform size. The lipid PS is exposed on dying cells and is considered to be an important eat-me signal (Fadok et al., 1992). PS was previously shown to cause Draper phosphorylation (Tung et al., 2013), but multiple protein ligands for Draper also have been suggested (Kuraishi et al., 2009; Okada et al., 2012). Based upon these prior studies, it was unclear whether one or multiple ligands were needed to execute full engulfment. To determine whether PS alone might be sufficient to trigger Draper-mediated engulfment, we replaced apoptotic cells with 6.5-µm-diameter silica beads coated with a lipid bilayer containing 10% PS and 0.5% atto390-phycoerythrin (PE) lipid for visualization by microscopy (Fig. 1 C). Draper-GFP S2 cells engulfed ∼0.8 PS beads per cell, on average, after a 30-min incubation (Fig. S1 B), which was 50-fold higher than the ingestion of beads coated only with phosphatidylcholine (PC) alone. Control GFP transfected S2 cells also engulfed PS-coated beads approximately sevenfold less efficiently than the Draper-GFP transfected cells (Fig. S1 B). As bead diameter decreased, Draper-GFP transfected cells internalized more beads (Fig. S1 C). Overexpression of Shark-mCherry did not increase engulfment of 10% PS beads (Fig. S1 D). Draper-GFP S2 cells engulfed beads at 2.5% PS lipid content and showed increasing engulfment up to 12.5% PS (Fig. 1 C). The PS concentrations that promote engulfment of beads are within the physiological range present on dead and dying cells (Leventis and Grinstein, 2010). Thus, our S2 cell system is a simplified two-component platform that is dependent on (1) overexpression of the Draper receptor and (2) PS exposed on a lipid bilayer–coated bead.

Next, we examined the activation of Draper in the presence of 10% PS beads. Similar to the apoptotic cell, we found that Shark-mCherry colocalized with Draper-GFP at the interface between PS bead and the Draper-transfected S2 cell (Fig. 1 D). A strong pTyr signal was also found at this interface as well (Fig. S1 E). Collectively, these results demonstrate that PS ligation is sufficient to trigger Draper locally and transmit the signal from target to cytosol (Fig. 1 D), where Draper receptor tails are phosphorylated and recruit the kinase Shark.

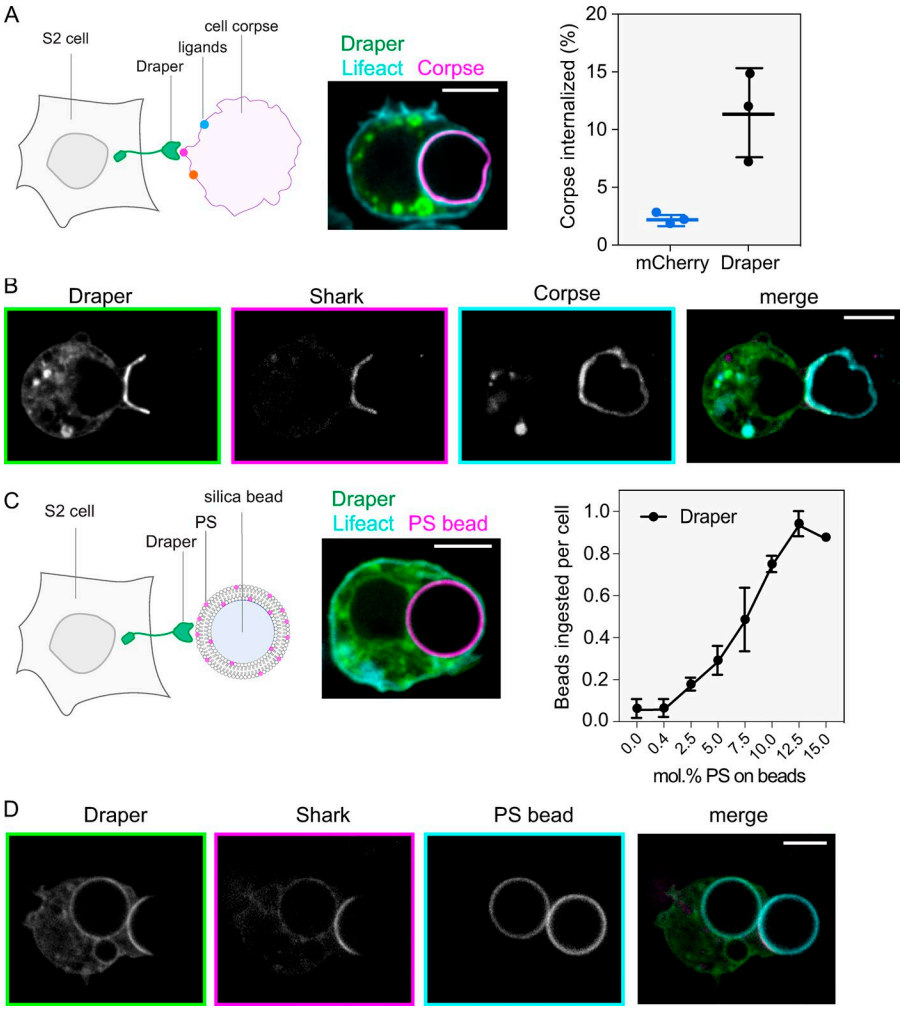

Figure 1. **Cellular reconstitution of Draper-dependent engulfment. (A)** Schematic of apoptotic cell clearance by Draper (green), which recognizes ligands to promote engulfment of cell corpses (purple). Representative image of an APC Annexin V–labeled cell corpse fully internalized by a Draper-GFP–expressing S2 cell. Overexpression of Draper-GFP in S2 cells results in an approximately fivefold increase in phagocytic proficiency toward apoptotic cell corpses. Draper-GFP$^+$ S2 cells were incubated with labeled cell corpses and phagocytic proficiency was assessed after a 45-min incubation at 27°C. Results from three independent biological replicates are shown (mean ± SD). **(B)** Draper-GFP's ability to bring Shark to the synapse between cell corpse (cyan) and S2 cell was assessed by live-cell imaging. Draper-GFP signal (left) overlaps with Shark-mCherry localization (middle) at the synapse between corpse and S2 cell. Shark was enriched in 13 of 13 synapses examined. **(C)** Schematic of reconstitution system to study Draper signaling. The cell corpse was replaced with a silica bead coated with a lipid bilayer containing PS. Representative image of an atto390-labeled 10% PS bead fully internalized by a Draper-GFP expressing S2 cell. Draper-GFP–expressing S2 cells were incubated with beads containing increasing mol % of PS in the lipid bilayer, and phagocytic proficiency was assessed after a 30-min incubation at 27°C. The number of beads fully ingested per cell for three independent biological replicates is shown (mean ± SD). **(D)** Shark kinase is enriched at the synapse between the 10% PS bead and the S2 cell. S2 cells were cotransfected with Draper-GFP and Shark-mCherry and incubated with 10% PS beads labeled with 0.5% atto390-DOPE. After 15 min, cells with active synapses were imaged by spinning-disk confocal microscopy. The middle slice from a z stack is shown. Shark was recruited to 26 of 30 synapses examined. Bars, 5 µm.

We next performed live-cell microscopy to visualize the process of Draper-mediated engulfment of PS beads (Fig. S1 F and Video 1). We cotransfected Draper-mCherry and LifeAct-GFP in S2 cells and imaged PS bead engulfment by time-lapse imaging. Draper-mCherry–expressing cells formed a synapse with PS beads and rapidly began forming a phagocytic cup; F-actin as assessed by LifeAct-GFP signal localized at the edges of the cup, and the leading edge of the cup extended gradually around the bead. When the phagocytic cup was complete, the PS bead was internalized. Thus, our system is useful for determining the kinetics of PS bead engulfment and following the dynamics of the cytoskeleton and membranes downstream of Draper activation.

Ligated Draper nucleates mobile microclusters that recruit effector proteins and remodel the actin cytoskeleton

To better visualize the behavior of Draper and the recruitment of proteins to the plasma membrane during the initiation of engulfment signaling, we used total internal reflection fluorescence microscopy (TIRF-M), a technique that confines illumination to within ∼200 nm of the glass coverslip. We coated the glass coverslip with a supported lipid bilayer (SLB) containing 10% PS (Fig. 2 A). When Draper-GFP S2 cells settled on this PS SLB, the cells spread rapidly on the surface in a futile effort to engulf the planar surface. Strikingly, Draper-GFP formed microclusters typically near the leading edge of the cell; these microclusters then underwent retrograde flow from the leading edge toward a central synapse at a rate of 1.42 ± 0.45 µm/min (mean ± SD, $n = 26$; Fig. 2 A and Video 2). The velocity of Draper-GFP microclusters was comparable with actin retrograde flow in this system (1.38 ± 0.40 µm/min; mean ± SD; $n = 25$). The behavior of these Draper clusters is very similar to that reported for adaptive immune receptor microclusters that form in B and T cells and are thought to serve as sites of local signal activation (Kaizuka et al., 2007; Murugesan et al., 2016).

Next, we asked whether Draper-GFP clusters are sites of recruitment for downstream signaling molecules. Draper is proposed to interact with Shark, a dual SH2 protein, and work with the adapter protein Crk, which harbors one SH2 domain and two SH3 domains. To test whether these proteins are recruited to Draper microclusters, we allowed Draper-GFP–, Shark-TagBFP–,

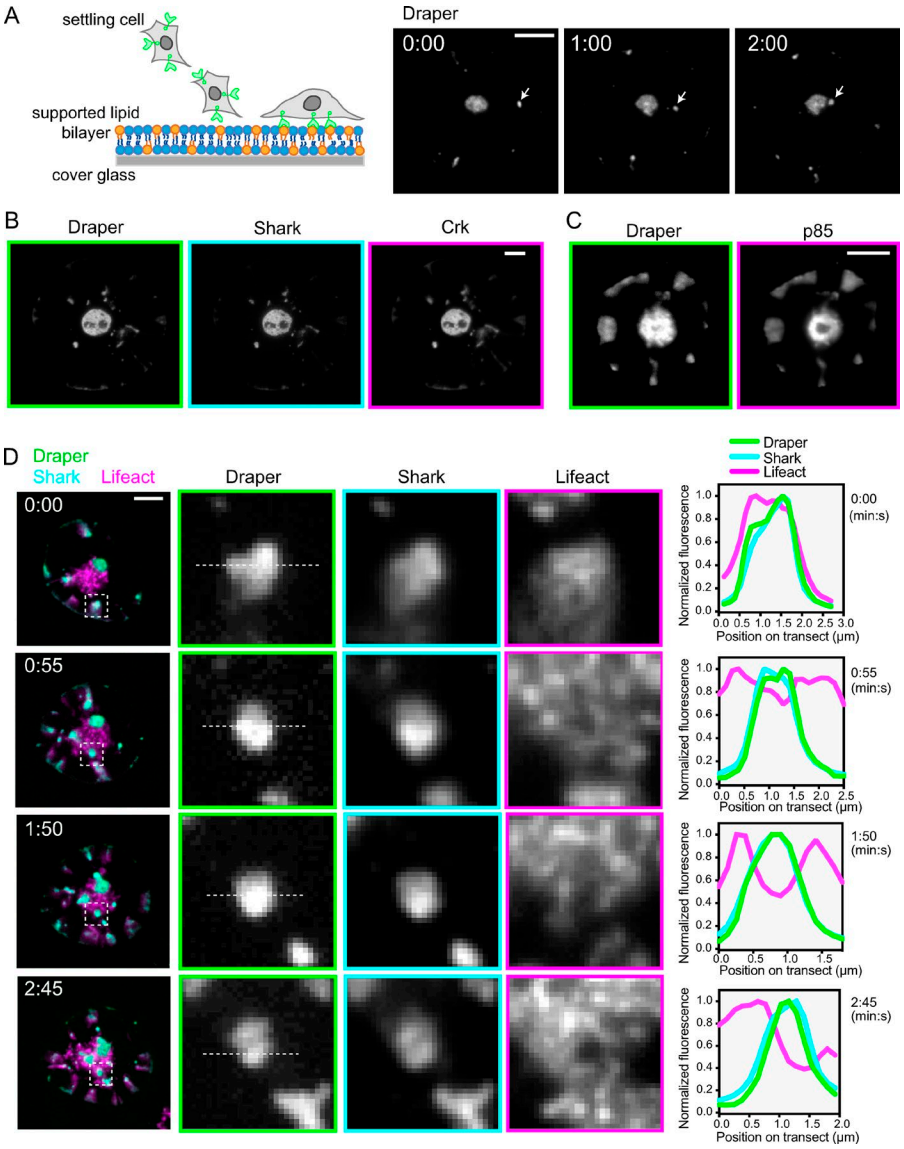

Figure 2. **Ligated Draper nucleates mobile microclusters that recruit effector proteins and remodel the actin cytoskeleton. (A)** Schematic of TIRF-M assay setup to visualize ligated Draper-GFP at the plasma membrane. Draper-GFP$^+$ S2 cells were allowed to settle on 10% PS SLBs prepared on a glass coverslip before imaging, and Draper-GFP$^+$ was imaged directly in real time. Draper-GFP forms microclusters on 10% PS SLBs. Draper-GFP microclusters visualized by TIRF-M undergo retrograde flow toward a central synapse of Draper-GFP. Microclusters fuse with one another and are repopulated from the periphery. The white arrows indicate the position of the same microcluster undergoing migration toward the central synapse over time. Time in minutes:seconds. Mobile microclusters were observed in 34 of 38 cells examined. **(B)** Draper-GFP microclusters on 10% PS bilayers recruit Shark-TagBFP and Crk-mCherry to the plasma membrane. Cells cotransfected with receptor, kinase, and adapter were allowed to settle on 10% PS bilayers and imaged after settling and spreading on the SLB. Draper-GFP, Shark-TagBFP, and Crk-mCherry colocalized in 14 of 14 spread cells examined. **(C)** Draper-mCherry microclusters on 10% PS bilayers recruit the activating subunit of PI3K (p85-GFP) to the plasma membrane. Cells cotransfected with Draper-mCherry and p85-GFP were allowed to settle on 10% PS bilayers as above and imaged after spreading. Draper-mCherry and p85-GFP colocalized in 20 of 21 cells examined. **(D)** Draper-GFP microclusters on 10% PS bilayers recruit Shark-mCherry but exclude the F-actin reporter LifeAct-TagBFP in a time-dependent manner. Cells cotransfected with Draper-GFP and LifeAct-TagBFP were allowed to settle and spread on 10% PS bilayers as above and imaged at 55-s intervals. The white box on the image at left highlights the expanded region at right to demonstrate that peripheral Draper-GFP microclusters colocalize with Shark-mCherry and LifeAct-TagBFP initially and appear to locally deplete F-actin over time as indicated by reduced LifeAct-TagBFP signal as the cluster matures over time. Transect showing position of plotted normalized fluorescence is indicated as a dashed line. Time in minutes:seconds. LifeAct-TagBFP depletion at Draper-GFP clusters was observed in 26 of 27 spread cells examined. Bars, 5 µm.

and Crk-mCherry–transfected S2 cells to settle on 10% PS bilayers and imaged them by TIRF-M. Activated Draper colocalized with Shark kinase, the adapter Crk, and the activating subunit of PI3K, p85 (Fig. 2, B and C; Fig. S2; and Video 3). Cytosolic pTyr-binding proteins colocalized with Draper at peripheral microclusters immediately upon formation and persisted during migration toward the large central synapse (Fig. 2, B and C). Collectively, these results demonstrate that upon ligation to PS, Draper is phosphorylated and nucleates formation of signaling microclusters, mobile assemblies that recruit multiple SH2-domain–containing proteins.

To determine whether Draper clusters have local effects on the actin cytoskeleton, we coexpressed Draper-mCherry, Shark-GFP, and LifeAct-BFP and allowed these cells to settle on PS bilayers. The appearance of Draper-mCherry microclusters was accompanied by an almost simultaneous colocalization signal with SharkGFP and LifeAct-BFP (Fig. 2 D; first time point, 0:00). Surprisingly, over time and while undergoing retrograde transport, the Shark-GFP signal remained consistently strong, while the LifeAct-BFP signal became depleted under the microcluster (Fig. 2 D and Video 4). These results suggest that Draper signaling temporally downstream of receptor phosphorylation leads to highly localized depletion of actin filaments. We observed a similar phenomenon at the synapse between Draper-GFP–expressing cells and PS beads (Fig. S3 A). To determine whether actin depletion contributes to the initial steps of signaling or the

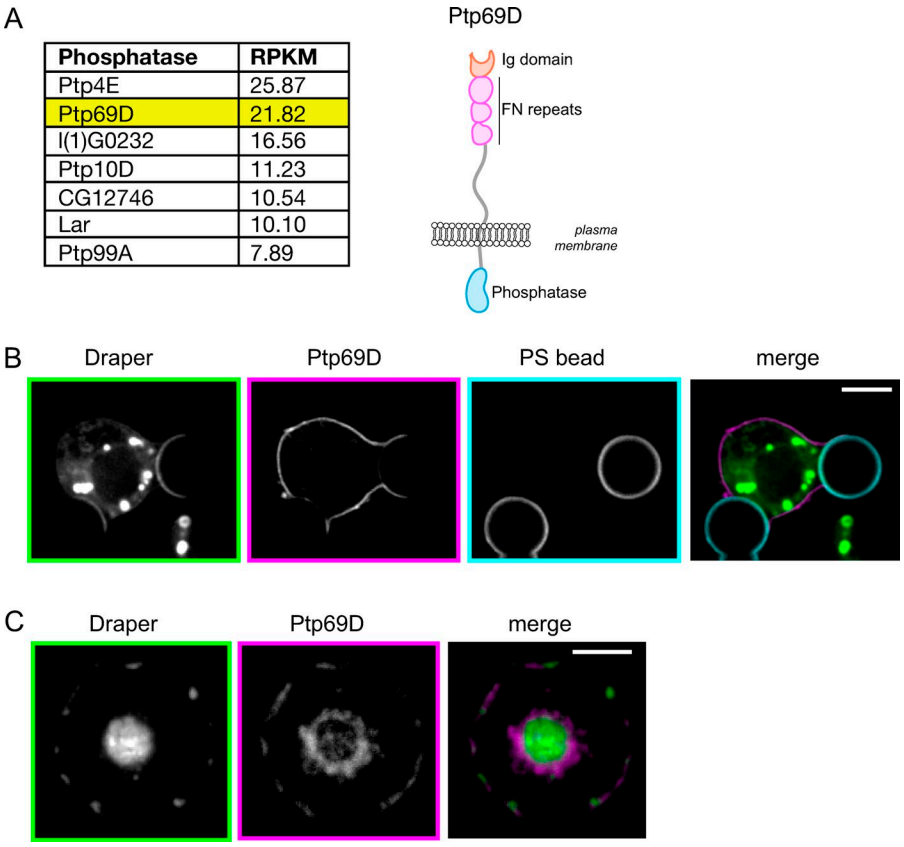

Figure 3. **Exclusion of a transmembrane phosphatase at the ligated membrane–membrane interface. (A)** S2 transmembrane phosphatase expression data and schematic of Ptp69D-GFP domain structure highlighting features of its bulky extracellular domain. Phosphatase expression levels are indicated in reads per kilobase of transcript, per million mapped reads (RPKM). FN, fibronectin. **(B)** The transmembrane phosphatase Ptp69D segregates away from Draper at synapses between 10% PS beads and the S2 cell. Draper-mCherry and Ptp69D-GFP were cotransfected into S2 cells and localization at the synapse with 10% PS beads assessed after a 15-min incubation. Ptp69D-GFP was excluded from 22 of 24 synapses examined. **(C)** Draper-mCherry clusters exclude Ptp69D-GFP on 10% PS SLBs. Draper-mCherry/Ptp69D-GFP–expressing S2 cells were allowed to settle and spread on bilayers and localization of receptor and phosphatase assessed after 15 min. Ptp69D-GFP exclusion from Draper-mCherry was observed in 22 of 25 spread cells examined. Bars, 5 µm.

process of engulfment, we treated cells with the synthetic actin nucleator jasplakinolide and scored assembly of phagocytic cups. Jasplakinolide-treated cells showed a striking defect in cup formation (Fig. S3 B), indicating that disruption of actin dynamics hinders early steps of Draper-dependent engulfment.

Exclusion of a transmembrane phosphatase at the ligated membrane–membrane interface

We next used our reconstitution system to define how PS triggers Draper phosphorylation. Both the TCRs and FcRs are believed to be triggered by the exclusion of the transmembrane phosphatase CD45, which has a bulky extracellular domain, from zones of close membrane–membrane contact created by the phosphorylated major histocompatibility complex (pMHC)-TCR or IgG-FcR binding (Choudhuri et al., 2005; Burroughs et al., 2006; James and Vale, 2012; Freeman et al., 2016). In contrast, Src family kinases associate with the inner leaflet of the plasma membrane via a palmitoylation and remain uniformly distributed after pMHC-TCR engagement. As a result, phosphatase exclusion shifts the kinase–phosphatase balance toward net receptor phosphorylation. In contrast, EGF receptor and G protein–coupled receptors are triggered via receptor conformational change (Dawson et al., 2005; Erlandson et al., 2018). We sought to determine which mechanism governs Draper triggering. The segregation model makes two key predictions: (1) a phosphatase with a bulky extracellular domain should be excluded from phosphorylated receptor microclusters, and (2) bringing the target membrane and phagocyte membrane into close proximity via a heterologous interaction module should trigger receptor phosphorylation and signaling. We sought to test whether a segregation mechanism might function to trigger Draper phosphorylation. *Drosophila* S2 cells express several transmembrane phosphatases as measured by RNA sequencing (Fig. 3 A; Zhang et al., 2010). We tested the transmembrane phosphatase Ptp69D because of its high expression level and similar domain structure to the segregated mammalian phosphatase CD45 (extracellular fibronectin repeats and cytosolic Try phosphatase activity; Fig. 3 A).

To determine whether Ptp69D segregates away from Draper at the ligated interface, we cotransfected the two proteins with different fluorescent protein tags and assessed localization in living cells. Microscopy revealed that ligated Draper-mCherry concentrated at the synapse between the S2 cell and PS bead, while Ptp69D-GFP was partially excluded from this zone (Fig. 3 B). Draper microclusters that formed at the interface between an S2 cell and a planar PS-containing SLB also excluded Ptp69D as visualized by TIRF-M (Fig. 3 C). Thus, Ptp69D segregates away from ligated Draper, a result that is consistent with a kinetic segregation triggering mechanism.

A synthetic receptor promotes Draper-dependent engulfment and actin remodeling

In the kinetic segregation model, two opposing membranes are brought into close apposition by the binding energy between receptor and its ligand, which results in the exclusion of larger transmembrane phosphatases (James and Vale, 2012; Cordoba et al., 2013; Carbone et al., 2017). To further examine whether Draper may trigger phosphorylation through a kinetic segregation mechanism rather than a receptor conformational change,

we tested whether the extracellular domain of Draper and its ligand PS could be replaced with an artificial receptor–ligand pair. Previous research on TCR triggering showed that the extracellular domain of the TCR and pMHC could be substituted with FKBP and FRB, which upon addition of rapamycin to bridge FKBP and FRB, trigger TCR phosphorylation (James and Vale, 2012). We created a similar inducible system for Draper by replacing its endogenous extracellular domain with FRB (FRB-EXT-Draper-INT) and replacing PS with His_{10}-FKBP, which was bound to the lipid bilayer on the bead via a Ni-NTA–lipid (Fig. 4 A). In the absence of rapamycin, beads were engulfed at very low levels (0.003 beads per cell). However, in the presence of rapamycin, the engineered receptor promoted robust engulfment of FKBP-bearing beads (Fig. 4 A and Video 5). Live-cell microscopy revealed that the FRB-EXT-Draper-INT concentrated at the cell–bead interface and recruited Shark kinase, suggesting that the chimeric receptor, like Draper, is activated by Tyr phosphorylation (Fig. 4 B). Like Draper-GFP, FRB-EXT-Draper-INT excluded the phosphatase Pt-p69D-GFP (Fig. 4 C), consistent with a kinetic segregation-based triggering mechanism. Thus, a chimeric receptor that is designed to interact with a nonphysiological ligand is functional for local receptor triggering, phosphatase exclusion, and engulfment.

Using LifeAct-GFP–expressing cells, we also examined whether microclusters nucleated by the FRB-EXT-Draper-INT receptor locally deplete F-actin. Like Draper, the FRB-EXT-Draper-INT receptor and LifeAct colocalized in the TIRF field, but over 1 min, the F-actin signal became depleted under the microcluster, creating the appearance of a small actin hole (Fig. 4 D and Video 6). Collectively, our results using the engineered FRB-EXT-Draper-INT receptor indicate that formation of a ligated zone that excludes a transmembrane phosphatase is sufficient to trigger receptor phosphorylation, effector recruitment, and local F-actin depletion observed for Draper.

Ordered multisite Tyr phosphorylation is required for full Draper activation

We first sought to determine which Tyr residues are essential for Draper-dependent engulfment in our cellular reconstitution assay. The Draper tail domain contains an ITAM motif (YxxI/Lx_{6-12}YxxI/L), an NPxY motif thought to interact with CED-6 (Fujita et al., 2012), and 10 other Tyr residues, two of which are in close proximity to the transmembrane domain. First, we created a construct in which 11 of the 13 Tyrs were mutated to alanine (Draper-Ala11-GFP), leaving the two Tyrs that are immediately adjacent to the transmembrane segment intact, since they potentially could have a structural role. We then compared phagocytic proficiency of cells transfected with Draper-Ala11-GFP mutant with full-length Draper-GFP and GFP alone (endogenous background phagocytosis). Consistent with a role for Tyr phosphorylation on Draper to promote phagocytosis, Draper-Ala11-GFP ingested PS beads at levels that were comparable with the GFP control and ∼15-fold below Draper-GFP cells after a 45-min incubation (Fig. 5 A).

We next sought to dissect the roles of Draper's cytoplasmic Tyr residues directly using a purified biochemical system on liposomes. The cytoplasmic tail of Draper and its cognate Src family *Drosophila* kinase Src42a (Ziegenfuss et al., 2008) were purified and bound via a His10 tag to Ni-NTA–modified lipids in the liposome. To detect binding between Shark and Draper, we used a fluorescently labeled tandem SH2 Shark construct (BG505-tSH2-Shark), whose signal quenches upon binding to Draper as it comes in proximity to a lipid-bound acceptor dye (Hui and Vale, 2014). After ATP was added as substrate for Src42a-mediated phosphorylation, we observed a time-dependent quenching of Shark fluorescence as it bound to the phosphorylated receptor (Fig. 5 B, orange trace). Next, we tested the Draper receptor with double Tyr to phenylalanine mutation in its ITAM motif (Fig. 5 B, Draper-ΔITAM). Draper-ΔITAM showed little or no recruitment of Shark (Fig. 5 B, blue trace). This biochemical result confirms that Shark binds Draper directly via Draper's ITAM (Ziegenfuss et al., 2008).

We next tested the role of the Draper ITAM in our cell-based system by mutating its two Tyr residues to Phe (Draper-ΔITAM; residues in Fig. 5 B) and assessed the ability of this mutant to promote phagocytosis. Draper-ΔITAM showed a kinetic delay and a lower number of beads ingested (Fig. 5 C) compared with WT Draper, revealing its critical role in signaling and Shark recruitment (Fig. S4). However, Draper-ΔITAM still promoted phagocytosis to a greater extent than the effectively null Draper-Ala11 construct (Fig. 5 C).

We also tested whether Draper's ITAM is sufficient to signal by adding back the ITAM Tyrs (Y934 and Y949) to the null Ala-11 mutant (Draper ITAM-only). The Draper ITAM-only receptor promoted phagocytosis of PS beads, but it did so more slowly than WT and to a lesser extent than WT Draper (Fig. 5 C). As expected, the Draper ITAM was necessary and sufficient to recruit Shark kinase to the synapse between S2 cell and PS bead (Fig. S4). Collectively, our mutational analyses suggest that Draper's ITAM plays a critical role in signaling but that non-ITAM residues also contribute to full receptor activity during engulfment.

To further understand the mechanism of Src42a-dependent activation of Draper, we tested the extent of Tyr phosphorylation on Draper's cytoplasmic tail in the on-membrane biochemical assay. After a 30-min kinase reaction, immunoblotting with anti-pTyr antibodies revealed a noticeable shift in the electrophoretic mobility of Draper, which is suggestive of phosphorylation on multiple Tyr residues (Fig. 5 D). Remarkably, even though the Draper-ΔITAM contains nine additional Tyr residues, its phosphorylation as detected by pTyr immunoblotting was minimal (5% of WT Draper) in the same kinase reaction (Fig. 5 D). We observed a similar result using the Src family kinase Lck (Fig. S5 A), suggesting that preferential modification through ITAM residues is a general mechanism of Draper receptor activation.

Greatly diminished phosphorylation of the Draper-ΔITAM mutant could arise because (1) only the ITAM residues are phosphorylated by Src family kinases or (2) phosphorylation of the ITAM motif is needed for the efficient phosphorylation of non-ITAM Tyrs in Draper's tail. To distinguish between these possibilities, we repeated the Draper phosphorylation assay and quenched reactions at 30 and 60 s after addition of ATP. To determine whether any residues on Draper are phosphorylated in ordered fashion, we performed 2D mass spectrometry on the 30- and 60-s samples. This method yielded peptides covering Tyr residues on Draper and allowed us to differentiate between

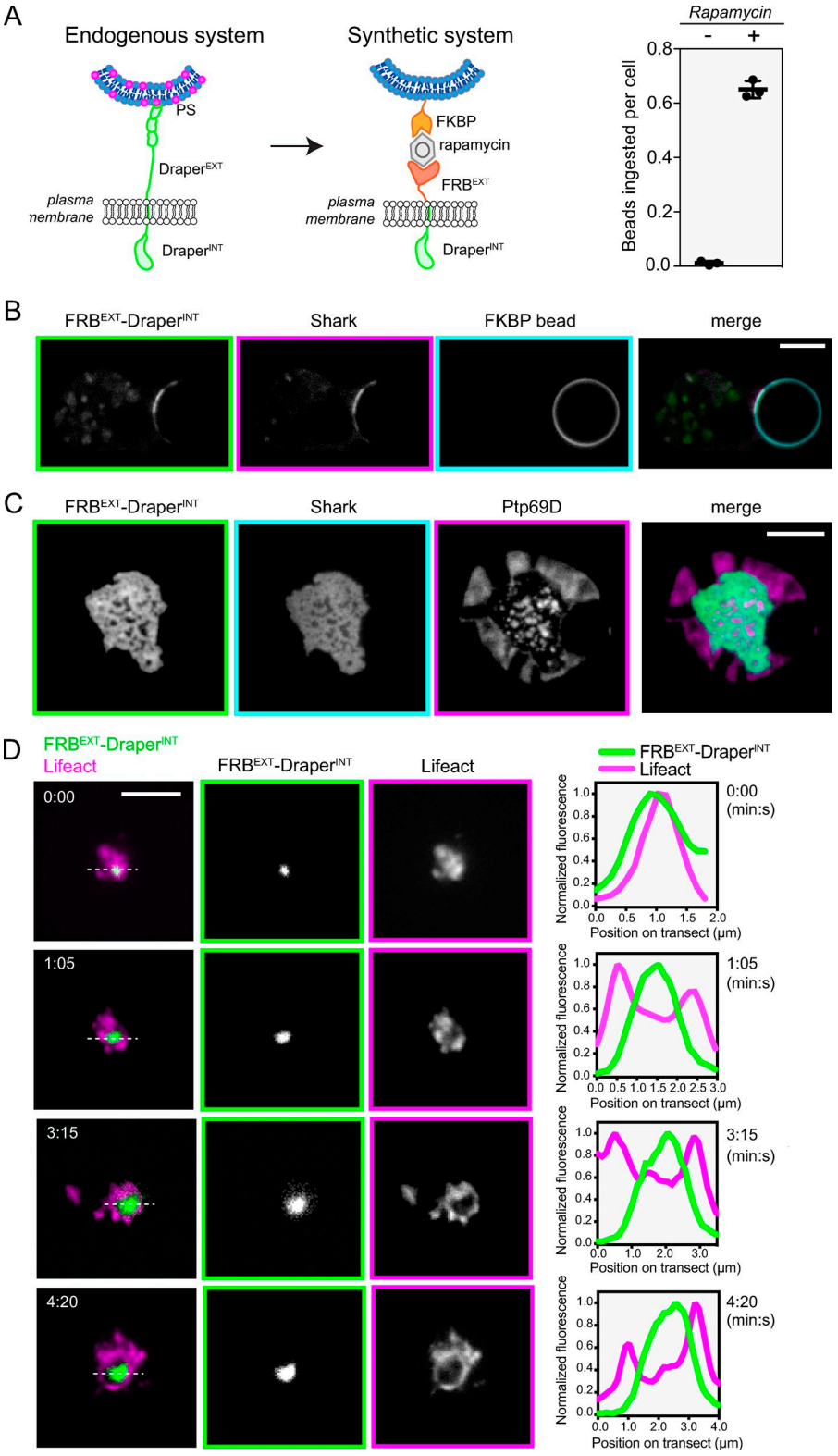

Figure 4. **A synthetic receptor promotes Draper-dependent engulfment and actin remodeling. (A)** Schematic showing extracellular FRB fused to the Draper transmembrane and cytosolic domains (FRB-EXT-Draper-INT) to program clearance signaling toward FKBP-bearing beads (see Materials and methods). FRB and FKBP are brought together into a 100 fM ternary complex in the presence of 1 µM rapamycin. FRB-EXT-Draper-INT promotes specific phagocytosis of FKBP beads. S2 cells transfected with FRB-EXT-Draper-INT were incubated with 10 nM FKBP beads for 30 min, after which bead ingestion was quantified after imaging using spinning-disk confocal microscopy (see Materials and methods). The number of beads fully ingested per cell for three independent biological replicates is shown (mean ± SD). Cells were incubated either with 1 µM rapamycin (right, +) or an equivalent volume of DMSO vehicle (left, –). **(B)** The kinase Shark is recruited to FRB-EXT-Draper-INT, indicating local receptor activation by Tyr phosphorylation. S2 cells expressing FRB-EXT-Draper-INT-GFP and Shark-Cherry were incubated with FKBP beads coupled to 10 nM his10 protein (see Materials and methods) in the presence of 1 µM rapamycin for 15 min and localization was assessed. A middle section from a confocal z stack is shown. Shark-mCherry was recruited to 18 of 18 synapses with FKBP beads examined. **(C)** S2 cells were transfected with FRB-EXT-Draper-INT-mCherry, Shark-TagBFP, and Ptp69D-GFP and allowed to settle on SLB with bound His_{10}-FKBP bilayers in the presence of 1 µM rapamycin for 15 min. Ptp69D segregates away from activated Draper at the interface between FKBP bilayer and S2 cell. In contrast, Draper and Shark overlapped, indicating a zone of local receptor activation and phosphorylation. Ptp69D-GFP was excluded from FRB-EXT-Draper-INT-GFP/Shark-TagBFP clusters in 42 of 42 cells examined. **(D)** FRB-EXT-Draper-INT microclusters on FKBP bilayers exclude the F-actin reporter LifeAct. Cells cotransfected with FRB-EXT-Draper-INT-mCherry and LifeAct-GFP were allowed to settle on His_{10}-FKBP bilayers as above and imaged at 65-s intervals. FRB-EXT-Draper-INT-mCherry microclusters colocalize with LifeAct-GFP initially and appear to locally deplete F-actin as indicated by reduced LifeAct-GFP signal as the cluster matures. Transect showing position of plotted normalized fluorescence is indicated as a dashed line. LifeAct-GFP segregation from FRB-EXT-Draper-INT-mCherry clusters was observed in 20 of 21 cells examined. Time in minutes:seconds. Bars, 5 µm.

phosphorylated and nonphosphorylated residues (Fig. 5 E). By comparing the proportion of phosphorylated peptides for each site at both 30 and 60 s, we could determine whether certain Tyr residues on Draper are preferentially modified over time. The ITAM Y934 residue was modified to a similar extent at both time points (pTyr ratio of 1.3; Fig. 5 E). However, the non-ITAM residues (except for Y888, which also had few phosphopeptides detected) were preferentially phosphorylated later as indicated by the 60:30-s ratios ranging from 1.9 to 5.2 (Fig. 5 E). Collectively, these results indicate that multiple Draper Tyrs are phosphorylated by Src42a and that phosphorylation of non-ITAM residues strongly depends on prior phosphorylation of the ITAM residues.

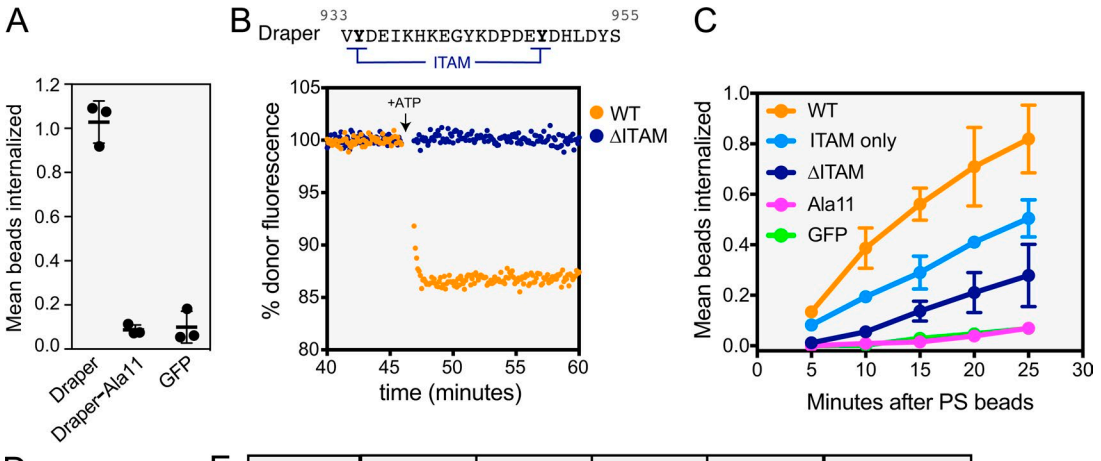

D

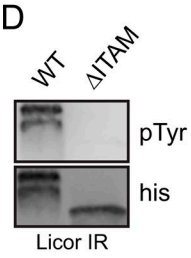

E

Tyr residue	pTyr 30 s	total 30 s	pTyr 60 s	total 60 s	pTyr ratio
838	0	0	0	0	not covered
858	0	0	0	0	not covered
888	**1**	**5**	**1**	**5**	**1.0**
901	**94**	**217**	**204**	**246**	**1.9**
905	**13**	**217**	**76**	**246**	**5.2**
924	**18**	**130**	**64**	**163**	**2.8**
934*	**53**	**111**	**94**	**155**	**1.3**
943	0	15	0	13	no pTyr
949*	0	17	0	15	no pTyr
954	0	17	0	15	no pTyr
965	0	0	0	0	no pTyr

Figure 5. **Ordered multisite Tyr phosphorylation is required for full Draper activation. (A)** Engulfment of 10% PS beads by S2 cells expressing Draper-GFP, Draper-Ala11-GFP, or a GFP control was assessed after a 45-min incubation. The number of beads ingested per cell for three biological replicates is shown (mean ± SD). **(B)** Alignment of residues mutated to Phe in Draper-ΔITAM. When a BG505-labeled reporter protein comes into close proximity to a rhodamine-labeled liposome, the 505-nm fluorescence signal is quenched. If quenching occurs after addition of ATP, it is most likely due to the Src42a-dependent phosphorylation of Draper's cytoplasmic Tyr residues and effector recruitment. The results shown in this panel reveal that direct binding of BG505-Shark-tSH2 to Draper's tail is dependent on an intact ITAM on Draper. His_{10}-Draper cytosolic domain or His_{10}-DraperY934F/Y949F (ΔITAM) receptor tail was ligated to 0.5% rhodamine-PE liposomes, and ATP-dependent quenching was assessed. **(C)** Draper-ΔITAM displays a kinetic delay and reduced phagocytic proficiency relative to Draper-GFP, while Draper's ITAM (ITAM only) is sufficient for partial engulfment activity. S2 cells transfected with Draper-GFP or the indicated mutants were incubated with 10% PS beads, allowed to settle, and imaged at the indicated time points. The number of beads fully ingested per cell for three independent biological replicates is shown (mean ± SD). **(D)** On-liposome phosphorylation reactions to assess Draper activation by its cognate Src family kinase Src42a. His_{10}-Draper cytoplasmic domain or 10×his-DraperY934F/Y949F (ΔITAM) receptor tail (both at 1 µM) were ligated to liposomes doped with DGS-Ni-NTA and incubated with 86 nM Src42a and 1 mM ATP for 30 min. Reactions were quenched with SDS-PAGE buffer containing DTT and 2-Me and boiled for 10 min at 95°C. Samples were immunoblotted with pTyr antibody or His_{10} antibody. Quantification of phosphorylation of WT or ΔITAM by Src42a was determined as the ratio of total pTyr signal over total His_{10} signal internally for each lane. Samples were visualized using Li-Cor infrared (IR) imaging. **(E)** 1 µM His_{10}-Draper cytoplasmic domain was phosphorylated using 1 nM on-membrane Src42a and samples quenched using 10 mM EDTA and 8 M urea. Reactions were digested for 2D mass spectrometry at 30-s and 60-s time points (see Materials and methods). 2D mass spectrometry peptide counts for each Tyr residue on Draper's cytoplasmic tail are shown. pTyr and total peptide counts for each time point are shown (30 s in blue and 60 s in red). pTyr in the right column indicates the ratio of (pTyr peptides at 60 s/all peptides) relative to the (pTyr peptides at 30 s/all peptides). A ratio above 1.0 indicates preferential phosphorylation at the later 60-s time point. "Not covered" indicates no peptides were detected for a residue in 2D mass spectrometry. "No pTyr" indicates that no peptides with the +79.9663 D shift characteristic of phosphorylation were detected. Asterisks indicate Tyr residues that compose the Draper ITAM.

Discussion

In this study, we converted poor phagocytes (*Drosophila* S2 cells) into proficient eaters by expressing a single receptor, Draper. We also show that PS is sufficient to locally trigger receptor phosphorylation and engulfment signaling, building on previous work that demonstrated PS-liposome–dependent Draper phosphorylation (Tung et al., 2013). Thus, we developed a simplified assay platform to dissect a complex cell signaling process that requires multiple receptors and ligands in vivo (Freeman and Grinstein, 2014). Draper is also reported to recognize the protein ligands Pretaporter and DmCaBP1 (Kuraishi et al., 2009; Okada et al., 2012) and has been reported to work in collaboration with coreceptors in flies such as Six Microns Under (Kurant et al., 2008) and integrins (Nagaosa et al., 2011). Our results do not rule out a role for these proteins in vivo to tune sensitivity for triggering and/or allow engulfment under low concentrations of PS (Manaka et al., 2004). However, our study shows that Draper interaction with PS provides a minimal system for studying apoptotic cell engulfment.

Using this cellular platform, in conjunction with a liposome-based biochemical assay, we have been able to gain insight into the initial steps of the corpse clearance signaling pathway

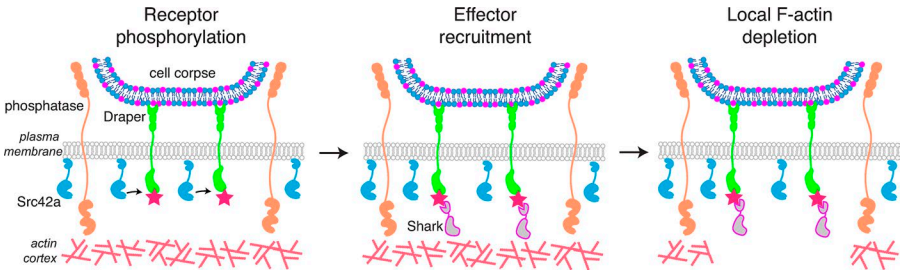

Figure 6. **Mechanism for engulfment signaling initiation.** Schematic representation of the early molecular steps of corpse clearance through the Draper receptor. Left: Draper ligation to PS on a cell corpse creates an exclusion zone where ligated receptors cluster at the synapse and unligated molecules such as bulky transmembrane phosphatases segregate away from receptors. Spatial segregation between receptors and inhibitory phosphatases shifts the balance toward receptor phosphorylation by Src42a. Middle: Tyr phosphorylation on Draper's tail recruits cytosolic effector proteins including the kinase Shark. Right: Effector recruitment promotes ordered signaling outputs including local depletion of F-actin at ligated microclusters.

(see model in Fig. 6). Our results show that ligation to the lipid PS is sufficient to promote Draper clustering and segregation of a transmembrane phosphatase at the ligated interface. Spatial separation between ligated Draper clusters and transmembrane phosphatases shifts a kinase–phosphatase balance in favor of receptor phosphorylation by Src42a. Phosphorylation of Draper's tail activates a downstream cytosolic signaling cascade, beginning with the recruitment of Shark and other pTyr-binding effector proteins, to Draper microclusters. After effector recruitment, early steps of Draper signaling include localized depolymerization of the actin cytoskeleton. Further downstream signaling likely leads to integrin activation and other events that lead to the formation of the phagocytic cup, although these more distal events in the pathway were not the focus of this study.

Comparison between Draper signaling and mammalian immune signaling

A potential similarity between Draper signaling and mammalian immune receptor activation was first suggested by the finding of an ITAM in the Draper cytoplasmic tail and the ability of this ITAM to bind Shark kinase in yeast two-hybrid and pulldown assays (Ziegenfuss et al., 2008). Our findings extend this work by providing evidence that Draper, like the T cell and Fc immune receptors, is triggered by a kinetic segregation mechanism. The kinetic segregation model, initially proposed as a mechanism for T cell activation, postulates that apposition of a membrane-membrane interface at the synapse between the T cell and antigen-presenting cell (APC) results in the exclusion of a bulky transmembrane phosphatase CD45, which shifts a kinase–phosphatase equilibrium in favor of receptor phosphorylation (Davis and van der Merwe, 2006). A segregation mechanism was recently proposed to regulate FcR activation, another mammalian immune signaling pathway, by creating an integrin-based diffusion barrier that excludes CD45 (Freeman et al., 2016).

Prior to our work, it remained unclear whether ligated corpse clearance receptors also use phosphatase exclusion to create zones of receptor triggering. In this study, we show that Draper ligation to PS on a second membrane excludes a transmembrane phosphatase (Ptp69D) from the synapse at the region of receptor phosphorylation and effector recruitment. Similar results showing exclusion were obtained with our chimeric receptor based on FKBP–rapamycin–FRB interaction. In the case of T cells, a single transmembrane phosphatase (CD45) is highly expressed on the surface and appears to be the dominant phosphatase in regulating signaling. However, phagocytic cells express several transmembrane phosphatases including Ptp69D, which together may contribute to regulating Draper and other phagocytic receptors. In the future, it will be illuminating to determine how the specific composition of phosphatases on the membrane (different sizes, localization patterns, and expression levels) are used to tune the sensitivity of engulfment and whether extracellular domains of differing sizes regulate engulfment as in other systems (Schmid et al., 2016; Carbone et al., 2017). It also will be interesting to explore whether Draper, like FcR (Freeman et al., 2016), activates integrin signaling to create a diffusion barrier for CD45.

Draper ligation to PS results in the formation of receptor microclusters, physical assemblies that organize engulfment effectors. The striking similarity extends to the recruitment of key signaling molecules to the microclusters. We show that similar to the TCR, Draper recruits several SH2-domain containing effector proteins, including Shark kinase, the adapter Crk, and the PI3K subunit p85. While the formation and retrograde transport of microclusters appears to be similar for the TCR and Draper, we observed a striking difference with regard to the effects of these clusters on F-actin. The TCR microclusters reside above actin-rich zones as they are transported from the periphery to the central supramolecular activation cluster (cSMAC) synapse (Kaizuka et al., 2007; DeMond et al., 2008; Yi et al., 2012; Murugesan et al., 2016). We also observed that Draper microclusters initially colocalize with the F-actin reporter LifeAct. However, as the clusters mature, but well before they reach the central synapse, the microclusters deplete F-actin to create "holes" in the actin cytoskeleton. We observed a similar anticorrelation between Draper and F-actin at microclusters of the synthetic FRB-EXT-Draper-INT receptor (Fig. 4 D) and at the large synapse between the Draper-expressing S2 cell and PS bead (Fig. S3 A). Our findings indicate that F-actin depletion over time both at peripheral microclusters and the central synapse is a distinct output of Draper receptor activation to actin regulators compared with the TCR signaling pathway.

Actin-depleted zones have been observed to form at the cSMAC at the mature synapse between a T cell and its target (Bunnell et al., 2001; Stinchcombe et al., 2001). For FcR-mediated engulfment, actin-depleted zones have been reported at the

interface between the phagocyte and a bead (Yamauchi et al., 2012; Schlam et al., 2015); actin depletion was suggested to be important for the phagocytosis of large, but not small, targets (Schlam et al., 2015). In addition, elegant recent work by Freeman et al. (2016) reported that macrophages interacting with micropatterned, immobilized IgG will polymerize F-actin surrounding the ligated FcRs, thereby forming actin rings. This study focused on integrin-mediated actin assembly at the periphery outside of the zone of receptor–ligand engagement, but images in Freeman et al. (2016) also reveal actin depletion at the center of the receptor zones in the micropatterned array.

The kinetics of actin depletion observed in this study suggests that actin depletion is an active part of the Draper signaling pathway that follows receptor phosphorylation by ∼1 min and is restricted to the zone of ligated receptors. The molecular mechanism responsible for actin disassembly could involve (1) a repression of Arp2/3 actin nucleation near the phosphorylated Draper receptor, potentially in combination with a barrier that presents nearby actin filaments from polymerizing or moving into the receptor zone; (2) RhoGAP repression of Rac and Cdc42 as suggested by Schlam et al. (2015) for large phagocytic cups; or (3) the recruitment and/or activation of actin-depolymerizing factors such as cofilin at the Draper signaling zone. Additional work will be needed to distinguish between these models.

Mechanism of Draper triggering upon ligation

The current model for T cell activation and FcR-mediated phagocytosis suggests that triggering is driven entirely by phosphorylation of ITAM Tyrs. In those cases, there are not additional Tyr residues outside of the ITAM motifs. Shark kinase, like ZAP70 and Syk, binds specifically to the ITAM motif on Draper, and we show that ITAM phosphorylation plays an important role in engulfment signaling. However, unlike the TCR and FcR, we show that Draper contains non-ITAM Tyrs that are also phosphorylated during activation and are functionally important for engulfment. We find that non-ITAM Tyrs play a role in Draper activation, thus supporting a signaling function both for Draper's ITAM and non-ITAM residues as suggested earlier (Ziegenfuss et al., 2008; Fujita et al., 2012). By measuring Draper Tyr phosphorylation directly via mass spectrometry, we report modification of residues outside of Draper's ITAM. Importantly, Draper's non-ITAM Tyr residues contribute to engulfment efficiency in cell-based assays. The phosphorylated non-ITAM Tyrs in Draper may bind additional SH2-containing adapter proteins or other effectors. Further studies will be needed to identify additional direct binding partners of the phosphorylated cytoplasmic tail domain of Draper and determine the higher-order structure of signaling microclusters that promote engulfment signaling.

Our biochemical reconstitution also reveals that Draper's ITAM domain is required for efficient phosphorylation of the non-ITAM Tyrs. This result indicates a sequential mechanism for multisite phosphorylation on Draper. One model for how this might occur is through the direct recruitment of Src family kinases to the phosphorylated ITAM domain of Draper. We show that the *Drosophila* Src42a kinase has a higher specificity for the Tyrs in Draper's ITAM domain and phosphorylates these residues first. We also confirmed ITAM specificity for Draper using Lck, another Src family kinase that phosphorylates ITAM domains on TCR cytosolic tails (Fig. S5 A). One possible mechanism for the sequential phosphorylation involves a mechanism in which a kinase creates its own binding site before modifying other residues. This idea has been suggested for Src-dependent phosphorylation of synthetic ITAM-containing substrate peptides (Pellicena et al., 1998) and phosphorylation of p130^{CAS} by Abl kinase (Mayer et al., 1995). A similar phenomenon was observed for Lck-dependent modification of sequential ITAM residues on the TCR, which is required for full activation of this receptor (Lewis et al., 1997). Thus, our data could be explained by Src42a binding to the phosphorylated ITAM through its own SH2 domain and then phosphorylating non-ITAM residues on Draper (Fig. 5). Thus, in common with other signaling systems, Draper phosphorylation involves a hierarchal phosphorylation of Tyrs in its tail domain, and this ordered sequence of phosphorylation events is required for full receptor activation.

Synthetic receptors to redirect engulfment signaling

We show in this study that the extracellular Draper–PS receptor–ligand pair can be functionally replaced by a synthetic inducible module, FKBP–rapamycin–FRB. The ability of this synthetic receptor to promote engulfment is analogous to findings for the TCR, which can be triggered using the same extracellular FKBP–rapamycin–FRB module (James and Vale, 2012). These programmed receptors enable activation of intracellular signaling pathways independently of their native extracellular domains. These synthetic receptors create signaling zones for both Draper (Fig. 4 C) and TCR (James and Vale, 2012) that exclude a transmembrane phosphatase to favor phosphorylation of intracellular receptor signaling domains. Inducible engulfment receptors consisting of intracellular receptor signaling tails fused to non-native extracellular domains are conceptually similar to chimeric receptors that trigger phagocytosis (Morrissey et al., 2018) and chimeric TCRs that recognize cancer antigen to promote specific cell killing (Lim and June, 2017). Collectively, these programmed signaling systems highlight the future promise of redirecting cells to target cancer, harmful debris, and pathogens.

Materials and methods

Reagents and recombinant DNA materials

The complete catalog information for reagents and tools used in this study can be found in Table S1. Detailed information for all recombinant DNA materials can be found in Table S2.

Drosophila S2 cell culture

Drosophila S2U cells were cultured in Schneider's media (Gibco) supplemented with 10% FBS (Atlanta) and 1× antibiotic/antimycotic (Gibco). S2 cells were grown in nonvented T25 or T75 flasks (Corning) and split every 3–6 d from high-density cultures (∼50–80%). S2U cells were not split to below ∼25% confluency as S2U cells are "unhappy" at low density. Healthy S2U cells adhere gently to the surface of the culture dish rather than floating but can be split by gently resuspending the adhered cells using a tissue culture pipet and a 10-ml sterile tissue culture pipet. Enzymatic dissociation using trypsin or by scraping

is unnecessary for S2U cells. Frozen stocks were prepared regularly. S2U freeze media contains 45% fresh complete media, 45% sterile filtered conditioned media prepared after spinning the media for 5 min at 1,000 *g*, and 10% DMSO (Sigma-Aldrich). A confluent T75 dish of S2U cells was pelleted for 5 min at 1,000*g*, resuspended in 10 ml freeze media (described above), split as 1-ml aliquots in externally threaded cryotubes (Corning), stored at −80°C in a cell-freezing apparatus containing isopropyl alcohol, and transferred to long-term storage in liquid nitrogen (vapor phase). Cells were regularly tested for mycoplasma using the MycoAlert kit (Lonza).

Transfection of *Drosophila* S2U cells

Cells were split to ∼60% confluency into six-well tissue culture dishes 4–12 h before transfection. All transfection mixes were prepared in 5 ml low-retention polystyrene round-bottom tubes. To prepare transfection mixes, a maximum of 2.5 µg plasmid DNA was added to 300 µl serum-free Schneider's media and gently mixed. 5 µl TransIT-Insect (Mirus) was added to diluted DNA and gently mixed. At this point, the solution appears cloudy. Transfection mixes were incubated at room temperature for 15 min and added dropwise gently to the 6-well plate using a p1000 pipet. After dropwise addition of transfection mixes, the plate was gently shaken laterally to ensure even distribution of TransIT-DNA particles. Transfection efficiencies of at least 50% and up to 90% were regularly obtained using this method, which is an improvement compared with other transient transfection methods employed for *Drosophila* S2U cells.

All constructs used in this study express proteins of interest in S2U cells were under control of a pMT copper-inducible promoter. To induce expression in transfected cells, $CuSO_4$ was added from a 50 mM sterile stock in water to a final concentration of 250 µM (1:200 dilution from stock) 36–48 h after transfection. The timing of induction is important; at this later time point, we find expression levels to be lower and more uniform. At shorter time points (e.g., 12–24 h after transfection), transfection efficiency was lower, and expression levels in transfected cells were higher, as assessed by live-cell imaging of fluorescent proteins under control of the pMT promoter.

Preparation of APC Annexin V–labeled apoptotic cell corpses

To prepare labeled apoptotic cell corpses for use in internalization assays, 1 µM final concentration of actinomycin D (1 mg/ml in DMSO; 833 µM stock; Sigma-Aldrich) was added directly to 80% confluent cultures of *Drosophila* S2U cells in 6-well plates. Cells were incubated for 16 h in actinomycin D before harvesting by centrifugation for 5 min at 1,000 *g* in a 15-ml falcon tube. Actinomycin D was washed out by rinsing corpses twice in complete Schneider's media in the same falcon tube; sequential washes, each with 10 ml complete media, were performed. Corpses from one well of a six-well dish were resuspended in 300 µl complete media after washes and transferred to a 1.7-ml Eppendorf tube for labeling. To label externalized PS, APC Annexin V (BioLegend) was added directly to the washed corpses to a final concentration of 50 ng/µl (from 5 µg/ml stock). The tube was wrapped in foil before labeling on a rotator at room temperature for 30 min. After labeling, cells were washed three times by sequential harvesting and resuspension in complete media. After washing, labeled corpses were resuspended in 300 µl complete media.

Assay for internalization of apoptotic cell corpses

To assess internalization of apoptotic cell corpses, washed Draper-GFP or mCherry-control transfected S2U cells were incubated with fresh complete media containing 10% FBS and labeled cell corpses prepared as above. Transfected cells were washed with complete S2U media, and culture media was replaced with 1 ml fresh complete culture media. Cells in fresh media were gently resuspended by pipetting up and down. 10 µl washed labeled cell corpses prepared as above was mixed in an Eppendorf tube with 300 µl washed transfected cells. The Eppendorf tube was flipped up and down four times, and complete mixture was plated in one well of a 96-well glass-bottom MatriPlate imaging dish (Brooks). After a 45-min incubation at room temperature in the dark, high-content screening imaging and quantification were performed as described below.

Preparation of 10% PS-coated silica beads

10 molar percent PS beads were used for all experiments other than the PS titration in Fig. 1 C. To prepare 10 molar percent beads, chloroform suspended lipids sufficient for 1 ml of a 10 mM solution were mixed at the following proportions: 89.5% POPC, 10% DOPS, 0.5% PEG5000-PE, and 0.5% atto390-DOPE (label for visualization by microscopy). Lipids were transferred to a chloroform-washed glass vial using gas-tight Hamilton syringes and dried to a film under argon gas in a warm (∼45°C) water bath. Dried lipids were stored under foil (if labeled lipids were used) and desiccated overnight at room temperature in a benchtop desiccator filled with Drierite. Dried lipids were suspended in 1 ml tissue culture–grade PBS by vortexing for 1 min under parafilm and gentle pipetting. Suspended lipids were transferred to a 1.7-ml Eppendorf tube and stored under argon gas. The PBS-lipid mix was freeze/thawed five times in liquid nitrogen and warm water and subjected to 2 × 5-min sonication in a Bioruptor Pico bath sonicator (Diagenode). Sonicated lipids were spun at 35,000 rpm for 35 min at 4°C in a TLA 120.1 rotor in a benchtop Beckman ultracentrifuge. Only a small pellet should be visible after spinning sonicated lipids. Small unilamellar vesicles (SUVs) prepared using this method were used immediately or stored under argon gas, flash frozen, and stored at −80°C. Lipid mixes are best used within 2 wk of preparation. Undiluted 10 mM lipid mixes were used as described below to build bilayers on silica beads. For the PS titration in Fig. 1 C, differences in PS concentration were made up by balanced changes to the molar percentage of PC such that final lipid concentration in 1 ml PBS matched the 10 mM concentration described above.

50 µl of 6.46-µm silica beads (SS06N; Bangs Labs) were added to 300 µl Milli-Q water in 1.7 ml Eppendorf tubes for washing. Beads in suspension were pelleted three times in 300 µl Milli-Q water at 300 rcf and decanted. After the third wash, beads were resuspended in ∼30 µl PBS until the pellet was barely covered. 300 µl of 2 mM final concentration of the desired lipid mix (diluted from 10 mM stock in PBS) was vortexed briefly, wrapped in foil, and rotated at room temperature for 45 min. Beads were pelleted and washed three times by sequential pelleting and

resuspension in 300 µl fresh PBS. Washed beads were resuspended in 300 µl fresh PBS for the bead assay (described below).

Assay for internalization of PS-coated silica beads

To assess internalization of PS-coated silica beads, 7 µl bead suspension was mixed with 300 µl washed transfected S2U cells resuspended in fresh complete media containing 10% FBS and flipped gently to mix four times, and then the complete mixture plated in one well of a 96-well glass bottomed MatriPlate imaging dish (Brooks). Cells were allowed to settle and imaged as described below. For endpoint assays, quantification was performed on images taken 30 or 45 min after plating. For kinetic experiments, imaging was started 5 min after plating. Engulfment experiments were performed using S2U cells cotransfected with GFP or a GFP-fusion receptor protein, mCherry-CAAX (full-length mCherry-LEKMSKDGKKKKKKSKTKCVIM) for visualizing plasma membranes during quantification (described below), and 10% PS atto390-PE–labeled silica beads.

Assay for internalization of His_{10}-FKBP silica beads

Engulfment experiments using His_{10}-FKBP ligated beads were performed as above with the exception that FRB-EXT-Draper-INT-GFP–expressing S2 cells were cotransfected with mCherry-CAAX to serve as a specific receptor for the FKBP ligand. Silica beads were prepared as above with the exception that instead of the 10% PS lipid mix, the following lipid mix was used: 97% POPC, 2% DGS-NTA-nickel, 0.5% PEG5000-PE, and 0.5% atto390-DOPE. Beads were blocked for 15 min in 300 µl PBS + 0.1% wt/vol BSA. His_{10}-FKBP was diluted to 10 nM final concentration in PBS + 0.1% wt/vol BSA, and 300 µl of this dilution was added to each 50-µl bead pellet as described above. Proteins were coupled to beads for 40 min under foil on a rotator at room temperature, washed 3 × 5 min in PBS + 0.1% wt/vol BSA, and resuspended in PBS + 0.1% wt/vol BSA before the engulfment assay. 300 µl washed transfected cells were mixed with 7 µl His_{10}-FKBP ligated beads either in the presence of 1 µM rapamycin or a matching volume of DMSO (vehicle) and flipped four times to mix, and ingestion was quantified as described below.

Staining for pTyr and the synapse between S2 cell and bead

To fix and stain bead–cell synapses in chambers described above for pTyr localization, half the media (~150 µl) from imaging chambers was gently removed and replaced with 150 µl of 6.4% paraformaldehyde. Cells were fixed under foil for 15 min, washed 2 × 3 min in PBS, permeabilized with 0.5% vol/vol Triton X-100 in PBS for 10 min, and set overnight to block in PBS + 0.1% vol/vol Triton X-100 + 0.2% wt/vol BSA at 4°C wrapped in parafilm in the dark. Cells were stained in primary antibody (pY-20 mouse anti-pTyr, 2 µg/ml final concentration, 1:100 dilution; Santa Cruz Biotechnology) for 1 h at room temperature in the dark, washed 3 × 5 min at room temperature in PBS + 0.1% vol/vol Triton X-100 + 0.2% wt/vol BSA, and incubated in secondary antibody (anti-mouse IgG H+L Alexa Fluor 647 conjugated; Thermo Fisher Scientific) for 1 h at room temperature, and washed 3 × 5 min in PBS + 0.1% vol/vol Triton X-100 + 0.2% wt/vol BSA. Washed fixed stained cells were gently covered in 200 µl PBS before imaging. Cells were imaged immediately or stored for up to 2 d at 4°C in the dark while wrapped in parafilm before imaging by spinning-disk confocal microscopy (see below).

Staining for endogenous Draper and Draper-GFP

To fix and stain for endogenous Draper localization versus the Draper-GFP construct, half the media (~150 µl) from imaging chambers was gently removed and replaced with 150 µl of 6.4% paraformaldehyde. Cells were fixed under foil for 15 min, washed 2 × 3 min in PBS, permeabilized with 0.5% vol/vol Triton X-100 in PBS for 10 min, and blocked for 20 min in PBS + 0.1% vol/vol Triton X-100 + 0.2% wt/vol BSA at room temperature. Cells were stained in primary antibody (8A1 Hybridoma supernatant; 1:2 final dilution overnight at 4°C; DSHB) washed 3 × 5 min room temperature in PBS + 0.1% vol/vol Triton X-100 + 0.2% wt/vol BSA, incubated in secondary antibody (anti-mouse IgG H+L Alexa Fluor 647 conjugated; Thermo Fisher Scientific) for 1 h at room temperature, and washed 3 × 5 min in PBS + 0.1% vol/vol Triton X-100 + 0.2% wt/vol BSA. Washed, fixed, and stained cells were gently covered in 200 µl PBS before imaging. Cells were imaged immediately by spinning-disk confocal microscopy (see below).

Building PS-containing SLBs

The night before the experiment, a 96-well MatriCal imaging plate was submerged in 2% vol/vol Hellmanex III, microwaved for 2.5 min on full power, and set on a stir plate under Saran wrap for at least 12 h. Hellmanex was washed away through 20 sequential washes using Milli-Q water and the washed plate dried under nitrogen gas. The dried plate was covered in thermal paper using a roller. The desired number of wells were exposed using a razor and washed 3 × 5 min in 5 N NaOH. After NaOH washes, wells were cleaned 10 times with Milli-Q water.

To prepare 10% PS bilayers, 250 µl of 2 mM lipid mix in PBS (described above) was gently pipetted on the glass surface. The lipid mix was pipetted up and down, and bilayer formation was allowed to proceed for 30 min at room temperature. After bilayers formed, 3 × 5 min washes were performed using PBS. For each wash, PBS was gently pipetted up and down over the surface of the bilayer to remove SUVs not part of the SLB. Bilayers were washed into serum-free Schneider's media before adding cells. Imaging on bilayers should be complete within 45 min for best results as bilayer integrity cannot be assumed after this time.

After washing the SLB, 150 µl of washed cells was added to the surface, allowed to settle, and imaged by TIRF-M as described below. A lower density of cells can be used as cells will spread on bilayers, and imaging overlapping cells is not ideal.

Building His_{10}-FKBP–bearing SLBs

Bilayers were prepared as above with the exception that the following lipid mix was used (note the use of DGS-NTA-nickel lipid to ligate His_{10} proteins to the bilayer): 97% POPC, 2% DGS-NTA-nickel, 0.5% PEG5000-PE, and 0.5% atto390-DOPE or 0.5% atto647-DOPE for labeling depending on the fluorescent proteins present on fusion proteins assessed. Washed bilayers were blocked in PBS + 0.1% wt/vol BSA for 15 min before protein coupling. To couple His_{10}-FKBP to 2% DGS-NTA–doped bilayers, His_{10}-FKBP was diluted to 10 nM final concentration in PBS + 0.1% wt/vol BSA and added to SLBs to couple for 40 min at room

temperature. Uncoupled protein was washed 3 × 5 min under foil at room temperature before adding cells as above with the exception that when FKBP ligand was used with receptors fused to FRB-extracellular domains, 1 µM rapamycin was added to form the 100 fM FRB–rapamycin–FKBP ternary complex.

Acute jasplakinolide treatment and quantification of phagocytic cup formation

S2 cells as above for bead internalization assay were treated with 1 µM final concentration jasplakinolide (a macrocyclic peptide that serves as an actin nucleator) or corresponding volume of DMSO (vehicle) for 20 min at room temperature. After acute drug treatment or control incubation, 7 µl of 10% PS bead suspension was mixed with the treated or control cells and flipped gently to mix four times, and then the complete mixture plated in one well of a 96-well glass-bottom MatriPlate imaging dish (Brooks). 15 min after plating, all cells exhibiting a synapse with one or more beads were scored for formation of phagocytic cups.

Liposome fluorescence resonance energy transfer assay for effector recruitment to phosphorylated receptor tails

This assay was based on one used to reconstitute mammalian T cell signaling (Hui and Vale, 2014). To present receptor tails in physiological geometry for phosphorylation by Src-family kinases, 1 µM His_{10} receptor tails (either His_{10}-Draper-INT or His_{10}-Draper-ΔITAM-INT) were ligated to liposomes comprised of the following molar percent: 74.5% POPC, 10% DGS-NTA, 0.5% rhodamine-PE, and 15% DOPS. Liposomes were prepared using an extruder with 200-nm filters (Avanti). Receptor tails and 1 nM His_{10}-Lck-Y505F or 86 nM Src42a (soluble) were equilibrated with receptor tails in the presence of BG505-kinase-tSH2 reporter proteins. Proteins were allowed to bind for 40 min at room temperature in the dark. At this point, Mg-ATP was added to a 1 mM final concentration, and BG505 signal was assessed at the indicated time points. Quenching of BG505 signal, dependent upon addition of ATP, indicates recruitment of reporters to phosphorylated receptor tails. Quenching of the BG505 dye was assessed using a Synergy H4 plate reader (BioTek).

Determining sites of Tyr phosphorylation by 2D mass spectrometry

To determine sites of Tyr phosphorylation on Draper (Fig. 5), 1 µM His_{10}-Draper-INT was ligated to unlabeled liposomes (74.5% POPC, 10% DGS-NTA, and 15% DOPS) and phosphorylated by 1 nM His_{10}-Lck-Y505F after 40 min of protein coupling to liposomes. 100-µl reactions were quenched with 100 µl of 8 M urea and 20 mM EDTA at the indicated time points (final concentrations of 4 M urea and 10 mM EDTA) and shock frozen in liquid nitrogen. To perform trypsinization, reactions were thawed by boiling, supplemented with a 5 mM final concentration of Tris(2-carboxyethyl)phosphine (TCEP), and incubated for 20 min at room temperature. After denaturation of samples, a 10 mM final concentration of iodoacetamide was added. Samples were then incubated in the dark for 15 min. Urea concentration was reduced twofold through addition of 200 µl PBS. A 1 mM final concentration of $CaCl_2$ and 1 µg/ml Trypsin Gold (Promega) was added before samples were incubated overnight in the dark at 37°C. Trypsinization was quenched through addition of 50 µl mass spectrometry–grade formic acid. Samples were then subjected to 2D mass spectrometry to remove contaminants, and peptides containing the characteristic shift for phosphorylation (+79.9663 D) were quantified and expressed as a percentage of all peptides covering the indicated residue.

Immunoblot analysis

To determine the degree of Tyr phosphorylation on His_{10}-Draper intracellular domains, liposome phosphorylation assays were performed as above, quenched using SDS-PAGE buffer + DTT, and incubated for 5 min at 95°C. Reactions were run on 4–20% gradient SDS-PAGE gels and transferred onto nitrocellulose membranes using the iBlot system (Invitrogen). Membranes were blocked for 1 h at room temperature in PBS + 0.1% wt/vol BSA (Sigma-Aldrich) and incubated overnight at 4°C with anti-His probe (rabbit) and anti-pTyr (mouse) antibodies (Table S1). Primary antibodies were incubated with membranes simultaneously. Both were used at 1:1,000 final dilution PBS + 0.1% wt/vol BSA. Membranes were washed 3 × 5 min at room temperature in PBS + 0.1% wt/vol BSA and incubated with Li-Cor secondary antibodies at 1:10,000 dilution (700 nm anti-rabbit and 800 nm anti-mouse; Table S1) for 1 h at room temperature. Membranes were washed 3 × 5 min at room temperature in PBS + 0.1% wt/vol BSA and imaged using a Li-Cor Odyssey gel imager. Quantification of anti-pTyr and anti-His intensity was performed using the Gel Analysis feature of Fiji (ImageJ; National Institutes of Health).

Protein expression, purification, and labeling

His_{10}-Draper and His_{10}-Draper-ΔITAM were transformed into BL-21 DE3 RIPL cells (Agilent). Cells were grown in Terrific Broth, 12 g tryptone, 24 g yeast extract, and 4 ml glycerol up to 1 liter in Milli-Q water + 10% vol/vol sterile salt solution in Milli-Q water (0.17 M KH_2PO_4 and 0.72 M K_2HPO_4) until cells reached an OD_{280} of ∼0.6–0.8, chilled in a 4°C room, and induced overnight by addition of 0.5 mM final concentration of IPTG. Protein expression was performed in shaker set to 18°C. Bacterial pellets were resuspended in lysis buffer (50 mM Hepes, pH 7.5, 300 mM NaCl, and 1 tablet Complete EDTA-free protease inhibitor tablet crushed per 100 ml buffer). Lysates were prepared by probe sonication and bound to Ni-NTA agarose (QIAGEN). Beads were washed extensively with lysis buffer, and proteins were eluted in 500 mM imidazole in lysis buffer. Imidazole elutions were subjected to gel filtration chromatography using a Superdex 200 10/30 column (GE Healthcare) in-gel filtration buffer (50 mM Hepes, pH 7.5, 150 mM NaCl, 10% glycerol, and 1 mM TCEP). Monomer fractions were pooled, shock frozen in liquid nitrogen, and stored in small aliquots at −80°C. Soluble Src42a was purified from SF9 cells as a GST-(PP)-SNAP-Src42a fusion, where PP indicates a cut site for PreScission Protease. PreScission Protease cleavage was performed overnight, and postcleavage supernatants were gel filtered as described below. His_{10}-Lck Y505F was purified from SF9 cells over nickel agarose (QIAGEN) and eluted in 500 mM imidazole in lysis buffer. His_{10}-Src42a was purified from *Escherichia coli* in the presence of GST-YopH to dephosphorylated the kinase. Imidazole elution was then run over GST resin (GE Healthcare) to remove the YopH phosphatase. All Src family

kinases were subjected to gel filtration chromatography using a Superdex 200 10/30 column (GE Healthcare) in gel filtration buffer (50 mM Hepes, pH 7.5, 150 mM NaCl, 10% glycerol, and 1 mM TCEP). Monomer fractions were pooled, shock frozen in liquid nitrogen, and stored in small aliquots at −80°C. The tandem SH2 domain reporter for Shark kinase was cloned as a GST-(PP)-SNAP-Shark-tSH2 fusion, where PP indicates a cut site for PreScission Protease. The soluble SNAP-Shark-tSH2 reporter was generated by on-resin cleavage with PreScission Protease during purification. GST-PreScission Protease remained on the beads. Cleavage products were subjected to gel filtration chromatography using a Superdex 200 10/30 column (GE Healthcare) in gel filtration buffer (50 mM Hepes, pH 7.5, 150 mM NaCl, 10% glycerol, and 1 mM TCEP). To prepare BG505-labeled SNAP-Shark-tSH2 for the liposome fluorescence resonance energy transfer assay, 10 µM cleaved, gel-filtered monomer was incubated at a 1:2 molar ratio with SNAP-Cell 505 Star (NEB) overnight in the dark at 4°C and run over a PD Minitrap G-25 column (GE Healthcare) to eliminate excess dye.

Spinning-disk confocal microscopy

All internalization and bead colocalization imaging performed for this study was done using a spinning-disk confocal microscope (Nikon Ti-Eclipse inverted microscope with a Yokogawa spinning disk). For bead internalization kinetic assays, images were acquired using a 40×/0.95 NA air objective. Live-image acquisition for internalization of corpses and beads was performed using the High Content Screening Site Generator plugin in µManager. All other images were acquired using a 100× 1.49 NA oil-immersion objective. Images were captured using an Andor iXon electron-multiplying charge-coupled device camera. The open source µManager software package was used to run the microscope and capture the images (Edelstein et al., 2010). All raw microscopy images were acquired as 16-bit TIFF stacks.

TIRF-M

All SLB imaging was performed using a TIRF microscope equipped with a motorized TIRF arm and a Hamamatsu Flash 4 camera. All TIRF-M imaging images were captured at 2 × 2 binning. The open-source µManager software package was used to run the microscope and capture the images (Edelstein et al., 2010).

Imaging processing and analysis

All image quantification was done on raw unprocessed images. All images in figures were opened in ImageJ. A middle z slice was extracted and the channels split. The image intensities were scaled to enhance contrast in Photoshop (Adobe) using appropriate levels of linear adjustment. Background correction was not performed. When mutants were compared in the same series, images were acquired using identical microscope and camera settings and scaled to equal intensity values.

Quantification and statistical analysis: Corpse and bead internalization assays

For both corpse internalization and bead internalization assays, targets were scored as internalized following complete engulfment of the object based on visible mCherry-CAAX or receptor-GFP signal visible completely around the target in stills from live imaging. Beads or corpses attached, but not internalized, were not scored as engulfed. Only targets with visible APC Annexin V (corpses) or attoPE lipid (beads) were scored as internalized. At least 100 cells per condition are shown. Mean ± 1 SD values are plotted (Prism 6.0; GraphPad Software).

Quantification and statistical analysis: Draper microcluster and actin retrograde flow velocities

Quantification of microcluster velocity was performed in MicroManager (Edelstein et al., 2010). Microcluster velocity was calculated by measuring the distance a single cluster traveled over a 100-s TIRF-M video captured at 5-s intervals. Quantification was performed on the same cell population used to calculate the velocity of actin retrograde flow (Draper-GFP; LifeAct-TagBFP transient transfection settling on 10% PS SLBs). A single channel (Draper-GFP) maximum-intensity z projection was created from a substack of 20 intervals. The freehand line tool was used to measure distance traveled by $n = 26$ microclusters on the maximum-intensity z projection. The reported velocity in the text is the mean for $n = 26$ individual microclusters; the microcluster velocity observed was 1.42 ± 0.45 µm/min (mean ± SD).

Quantification of actin retrograde flow velocity was performed in MicroManager (Edelstein et al., 2010). Quantification of actin retrograde flow was performed on the same cell population used to calculate the velocity of Draper microclusters above (Draper-GFP and LifeAct-TagBFP). To calculate actin retrograde flow, cells were spread on Concanavalin A so actin flow could be clearly visualized using TIRF-M. Actin retrograde flow velocities were calculated using a kymograph selected from the lamellar portion of the cell perpendicular to the leading edge. The reported velocity in the text is the mean for $n = 25$ individual measurements; the velocity observed was 1.38 ± 0.40 µm/min (mean ± SD).

Quantification and statistical analysis: Quantification of Draper, Shark, and LifeAct intensity

Quantification of normalized fluorescence intensity was performed in MicroManager (Edelstein et al., 2010). Intensity for each indicated channel was collected across a 2-pixel linescan for each indicated time point using the Plot Profile tool in ImageJ. Intensity measurements were performed in the same manner for TIRF-M and spinning-disk confocal imaging. Background was measured as the mean value for a 2-pixel linescan at a region adjacent to the cell. Background was subtracted from intensity at each position before normalization. Values were normalized to the maximum intensity across the linescan. Normalized intensity values are plotted using distance along the transect as the x axis. Transects are indicated on inset images for each cluster.

Quantification and statistical analysis: Quantification of Draper immunofluorescence intensity

Quantification of immunofluorescence intensity using the anti-Draper 81A antibody was performed in MicroManager (Edelstein et al., 2010). The data in Fig. S1 A represent the corrected total cell fluorescence (CTCF) values for each cell corresponding with the condition shown on the x axis.

CTCF = integrated density − (area of cell × mean background signal for the same image) for the 647 anti–mouse secondary antibody. We chose CTCF because it is an area-corrected analysis method that takes into account the background in each image.

Online supplemental material

The supplemental figures contain supporting microscopy images and information directly in support of the main-text figures. Full legends accompany each supplemental figure. Fig. S1 supports Fig. 1 by comparing the subcellular localization between endogenous Draper and Draper-GFP and showing the fold overexpression in the Draper-GFP transfection system. We also characterize the system by investigating the bead diameter dependence and Shark requirement. This figure further supports Fig. 1 by demonstrating both a Draper and PS dependence for efficient engulfment as well as initiation of pTyr signaling and projections around a PS bead. Fig. S2 supports Fig. 2 by showing that the engulfment effectors that localize to signaling microclusters are also recruited to Draper at the synapse with a 10% PS bead. Fig. S3 supports Fig. 2 by showing that actin depletion behavior is observed in the bead assay. This figure also supports Fig. 2 by demonstrating that disruption of actin dynamics using the drug jasplakinolide disrupts early steps of Draper-dependent engulfment. Fig. S4 supports Fig. 5 by demonstrating that Draper's ITAM is necessary and sufficient for Shark kinase recruitment in cells. Fig. S5 supports Fig. 5 by showing that like Src42a, the Src family kinase Lck preferentially modifies Draper based on the presence of an ITAM. This figure also supports Figs. 2 and 5 by showing that the N-terminal SH2 domain of p85 does not directly bind Draper's cytoplasmic tail in an on-liposome biochemical assay. The complete catalog information for reagents and tools used in this study can be found in Table S1. Detailed information for all recombinant DNA materials can be found in Table S2. Video 1 shows cellular reconstitution of Draper signaling. Video 2 shows formation of mobile Draper-GFP microclusters on 10% PS bilayers. Video 3 shows visualization of signaling microclusters on 10% PS bilayers. Video 4 shows split channel visualization of Draper, Shark, and F-actin on 10% PS bilayers. Video 5 shows visualization of FKBP-bead engulfment by a chimeric FRB-Draper receptor. Video 6 shows visualization of FRB-EXT-Draper-INT and LifeAct in an FKBP SLB.

Acknowledgments

We thank N. Stuurman for help with microscopy; and C. Carbone, E. Hui, N. Kern, M. Morrissey, X. Su, and M. Taylor for discussions. The following members of the Vale lab assisted with lipid reagents and experimental advice: E. Hui (University of California, San Diego, San Diego, CA), X. Su (Yale School of Medicine, New Haven, CT), and M. Taylor (Max Planck Institute for Infection Biology, Berlin, Germany). We thank L. Kohlstaedt and Y.-S. Kim (Vincent J. Coates Proteomics/Mass Spectrometry Laboratory, University of California, Berkeley, Berkeley, CA) for performing the mass spectrometry. We also thank K. McKinley, M. Morrissey, E. Hui, A. Jain, X. Su, T. Skokan, and P. Williamson for helpful critiques of the manuscript.

A.P. Williamson was supported by a Cancer Research Institute–Irvington Postdoctoral Fellowship. This work was funded by the Howard Hughes Medical Institute and the National Institutes of Health (5R35GM118106-02 to R.D. Vale). The Vincent J. Coates Proteomics/Mass Spectrometry Laboratory at University of California, Berkeley, is supported in part by the National Institutes of Health (S10 Instrumentation grant S10RR025622).

The authors declare no competing financial interests.

Author contributions: A.P. Williamson: conceptualization, methodology, validation, formal analysis, investigation, writing – original draft, writing – review and editing, visualization, and funding acquisition; R.D. Vale: conceptualization, methodology, resources, supervision, writing – review and editing, and funding acquisition.

Submitted: 27 November 2017
Revised: 25 March 2018
Accepted: 30 July 2018

References

Arandjelovic, S., and K.S. Ravichandran. 2015. Phagocytosis of apoptotic cells in homeostasis. *Nat. Immunol.* 16:907–917. https://doi.org/10.1038/ni.3253

Bunnell, S.C., V. Kapoor, R.P. Trible, W. Zhang, and L.E. Samelson. 2001. Dynamic actin polymerization drives T cell receptor-induced spreading: a role for the signal transduction adaptor LAT. *Immunity.* 14:315–329. https://doi.org/10.1016/S1074-7613(01)00112-1

Burroughs, N.J., Z. Lazic, and P.A. van der Merwe. 2006. Ligand detection and discrimination by spatial relocalization: A kinase-phosphatase segregation model of TCR activation. *Biophys. J.* 91:1619–1629. https://doi.org/10.1529/biophysj.105.080044

Carbone, C.B., N. Kern, R.A. Fernandes, E. Hui, X. Su, K.C. Garcia, and R.D. Vale. 2017. In vitro reconstitution of T cell receptor-mediated segregation of the CD45 phosphatase. *Proc. Natl. Acad. Sci. USA.* 114:E9338–E9345. https://doi.org/10.1073/pnas.1710358114

Cherbas, L., A. Willingham, D. Zhang, L. Yang, Y. Zou, B.D. Eads, J.W. Carlson, J.M. Landolin, P. Kapranov, J. Dumais, et al. 2011. The transcriptional diversity of 25 Drosophila cell lines. *Genome Res.* 21:301–314. https://doi.org/10.1101/gr.112961.110

Choudhuri, K., D. Wiseman, M.H. Brown, K. Gould, and P.A. van der Merwe. 2005. T-cell receptor triggering is critically dependent on the dimensions of its peptide-MHC ligand. *Nature.* 436:578–582. https://doi.org/10.1038/nature03843

Cordoba, S.-P., K. Choudhuri, H. Zhang, M. Bridge, A.B. Basat, M.L. Dustin, and P.A. van der Merwe. 2013. The large ectodomains of CD45 and CD148 regulate their segregation from and inhibition of ligated T-cell receptor. *Blood.* 121:4295–4302. https://doi.org/10.1182/blood-2012-07-442251

Davis, S.J., and P.A. van der Merwe. 2006. The kinetic-segregation model: TCR triggering and beyond. *Nat. Immunol.* 7:803–809. https://doi.org/10.1038/ni1369

Dawson, J.P., M.B. Berger, C.-C. Lin, J. Schlessinger, M.A. Lemmon, and K.M. Ferguson. 2005. Epidermal growth factor receptor dimerization and activation require ligand-induced conformational changes in the dimer interface. *Mol. Cell. Biol.* 25:7734–7742. https://doi.org/10.1128/MCB.25.17.7734-7742.2005

DeMond, A.L., K.D. Mossman, T. Starr, M.L. Dustin, and J.T. Groves. 2008. T cell receptor microcluster transport through molecular mazes reveals mechanism of translocation. *Biophys. J.* 94:3286–3292. https://doi.org/10.1529/biophysj.107.119099

Edelstein, A., N. Amodaj, K. Hoover, R. Vale, and N. Stuurman. 2010. Computer control of microscopes using μManager. *Curr. Protoc. Mol. Biol.* https://doi.org/10.1002/0471142727.mb1420s92

Elliott, M.R., and K.S. Ravichandran. 2010. Clearance of apoptotic cells: implications in health and disease. *J. Cell Biol.* 189:1059–1070. https://doi.org/10.1083/jcb.201004096

Erlandson, S.C., C. McMahon, and A.C. Kruse. 2018. Structural Basis for G Protein-Coupled Receptor Signaling. *Annu. Rev. Biophys.* 47. https://doi.org/10.1146/annurev-biophys-070317-032931

Etchegaray, J.I., A.K. Timmons, A.P. Klein, T.L. Pritchett, E. Welch, T.L. Meehan, C. Li, and K. McCall. 2012. Draper acts through the JNK pathway to

control synchronous engulfment of dying germline cells by follicular epithelial cells. *Development.* 139:4029–4039. https://doi.org/10.1242/dev.082776

Fadok, V.A., D.R. Voelker, P.A. Campbell, J.J. Cohen, D.L. Bratton, and P.M. Henson. 1992. Exposure of phosphatidylserine on the surface of apoptotic lymphocytes triggers specific recognition and removal by macrophages. *J. Immunol.* 148:2207–2216.

Freeman, S.A., and S. Grinstein. 2014. Phagocytosis: receptors, signal integration, and the cytoskeleton. *Immunol. Rev.* 262:193–215. https://doi.org/10.1111/imr.12212

Freeman, M.R., J. Delrow, J. Kim, E. Johnson, and C.Q. Doe. 2003. Unwrapping glial biology: Gcm target genes regulating glial development, diversification, and function. *Neuron.* 38:567–580. https://doi.org/10.1016/S0896-6273(03)00289-7

Freeman, S.A., J. Goyette, W. Furuya, E.C. Woods, C.R. Bertozzi, W. Bergmeier, B. Hinz, P.A. van der Merwe, R. Das, and S. Grinstein. 2016. Integrins Form an Expanding Diffusional Barrier that Coordinates Phagocytosis. *Cell.* 164:128–140. https://doi.org/10.1016/j.cell.2015.11.048

Fujita, Y., K. Nagaosa, A. Shiratsuchi, and Y. Nakanishi. 2012. Role of NPxY motif in Draper-mediated apoptotic cell clearance in Drosophila. *Drug Discov. Ther.* 6:291–297.

Hui, E., and R.D. Vale. 2014. In vitro membrane reconstitution of the T-cell receptor proximal signaling network. *Nat. Struct. Mol. Biol.* 21:133–142. https://doi.org/10.1038/nsmb.2762

Iram, T., Z. Ramirez-Ortiz, M.H. Byrne, U.A. Coleman, N.D. Kingery, T.K. Means, D. Frenkel, and J. El Khoury. 2016. Megf10 Is a Receptor for C1Q That Mediates Clearance of Apoptotic Cells by Astrocytes. *J. Neurosci.* 36:5185–5192. https://doi.org/10.1523/JNEUROSCI.3850-15.2016

James, J.R., and R.D. Vale. 2012. Biophysical mechanism of T-cell receptor triggering in a reconstituted system. *Nature.* 487:64–69. https://doi.org/10.1038/nature11220

Kaizuka, Y., A.D. Douglass, R. Varma, M.L. Dustin, and R.D. Vale. 2007. Mechanisms for segregating T cell receptor and adhesion molecules during immunological synapse formation in Jurkat T cells. *Proc. Natl. Acad. Sci. USA.* 104:20296–20301. https://doi.org/10.1073/pnas.0710258105

Kawano, M., and S. Nagata. 2018. Lupus-like autoimmune disease caused by a lack of Xkr8, a caspase-dependent phospholipid scramblase. *Proc. Natl. Acad. Sci. USA.* 115:2132–2137. https://doi.org/10.1073/pnas.1720732115

Kuraishi, T., Y. Nakagawa, K. Nagaosa, Y. Hashimoto, T. Ishimoto, T. Moki, Y. Fujita, H. Nakayama, N. Dohmae, A. Shiratsuchi, et al. 2009. Pretaporter, a Drosophila protein serving as a ligand for Draper in the phagocytosis of apoptotic cells. *EMBO J.* 28:3868–3878. https://doi.org/10.1038/emboj.2009.343

Kurant, E., S. Axelrod, D. Leaman, and U. Gaul. 2008. Six-microns-under acts upstream of Draper in the glial phagocytosis of apoptotic neurons. *Cell.* 133:498–509. https://doi.org/10.1016/j.cell.2008.02.052

Leventis, P.A., and S. Grinstein. 2010. The distribution and function of phosphatidylserine in cellular membranes. *Annu. Rev. Biophys.* 39:407–427. https://doi.org/10.1146/annurev.biophys.093008.131234

Lewis, L.A., C.D. Chung, J. Chen, J.R. Parnes, M. Moran, V.P. Patel, and M.C. Miceli. 1997. The Lck SH2 phosphotyrosine binding site is critical for efficient TCR-induced processive tyrosine phosphorylation of the zeta-chain and IL-2 production. *J. Immunol.* 159:2292–2300.

Lim, W.A., and C.H. June. 2017. The Principles of Engineering Immune Cells to Treat Cancer. *Cell.* 168:724–740. https://doi.org/10.1016/j.cell.2017.01.016

Lu, T.-Y., J. Doherty, and M.R. Freeman. 2014. DRK/DOS/SOS converge with Crk/Mbc/dCed-12 to activate Rac1 during glial engulfment of axonal debris. *Proc. Natl. Acad. Sci. USA.* 111:12544–12549. https://doi.org/10.1073/pnas.1403450111

MacDonald, J.M., M.G. Beach, E. Porpiglia, A.E. Sheehan, R.J. Watts, and M.R. Freeman. 2006. The Drosophila cell corpse engulfment receptor Draper mediates glial clearance of severed axons. *Neuron.* 50:869–881. https://doi.org/10.1016/j.neuron.2006.04.028

Manaka, J., T. Kuraishi, A. Shiratsuchi, Y. Nakai, H. Higashida, P. Henson, and Y. Nakanishi. 2004. Draper-mediated and phosphatidylserine-independent phagocytosis of apoptotic cells by Drosophila hemocytes/macrophages. *J. Biol. Chem.* 279:48466–48476. https://doi.org/10.1074/jbc.M408597200

Mayer, B.J., H. Hirai, and R. Sakai. 1995. Evidence that SH2 domains promote processive phosphorylation by protein-tyrosine kinases. *Curr. Biol.* 5:296–305. https://doi.org/10.1016/S0960-9822(95)00060-1

Morrissey, M.A., A.P. Williamson, A.M. Steinbach, E.W. Roberts, N. Kern, M.B. Headley, and R.D. Vale. 2018. Chimeric antigen receptors that trigger phagocytosis. *eLife.* 7:31. https://doi.org/10.7554/eLife.36688

Murugesan, S., J. Hong, J. Yi, D. Li, J.R. Beach, L. Shao, J. Meinhardt, G. Madison, X. Wu, E. Betzig, and J.A. Hammer. 2016. Formin-generated actomyosin arcs propel T cell receptor microcluster movement at the immune synapse. *J. Cell Biol.* 215:383–399. https://doi.org/10.1083/jcb.201603080

Nagaosa, K., R. Okada, S. Nonaka, K. Takeuchi, Y. Fujita, T. Miyasaka, J. Manaka, I. Ando, and Y. Nakanishi. 2011. Integrin βv-mediated phagocytosis of apoptotic cells in Drosophila embryos. *J. Biol. Chem.* 286:25770–25777. https://doi.org/10.1074/jbc.M110.204503

Neumann, B., S. Coakley, R. Giordano-Santini, C. Linton, E.S. Lee, A. Nakagawa, D. Xue, and M.A. Hilliard. 2015. EFF-1-mediated regenerative axonal fusion requires components of the apoptotic pathway. *Nature.* 517:219–222. https://doi.org/10.1038/nature14102

Okada, R., K. Nagaosa, T. Kuraishi, H. Nakayama, N. Yamamoto, Y. Nakagawa, N. Dohmae, A. Shiratsuchi, and Y. Nakanishi. 2012. Apoptosis-dependent externalization and involvement in apoptotic cell clearance of DmCaBP1, an endoplasmic reticulum protein of Drosophila. *J. Biol. Chem.* 287:3138–3146. https://doi.org/10.1074/jbc.M111.277921

Pellicena, P., K.R. Stowell, and W.T. Miller. 1998. Enhanced phosphorylation of Src family kinase substrates containing SH2 domain binding sites. *J. Biol. Chem.* 273:15325–15328. https://doi.org/10.1074/jbc.273.25.15325

Ravichandran, K.S., and U. Lorenz. 2007. Engulfment of apoptotic cells: signals for a good meal. *Nat. Rev. Immunol.* 7:964–974. https://doi.org/10.1038/nri2214

Reddien, P.W., and H.R. Horvitz. 2004. The engulfment process of programmed cell death in caenorhabditis elegans. *Annu. Rev. Cell Dev. Biol.* 20:193–221. https://doi.org/10.1146/annurev.cellbio.20.022003.114619

Scheib, J.L., C.S. Sullivan, and B.D. Carter. 2012. Jedi-1 and MEGF10 signal engulfment of apoptotic neurons through the tyrosine kinase Syk. *J. Neurosci.* 32:13022–13031. https://doi.org/10.1523/JNEUROSCI.6350-11.2012

Schlam, D., R.D. Bagshaw, S.A. Freeman, R.F. Collins, T. Pawson, G.D. Fairn, and S. Grinstein. 2015. Phosphoinositide 3-kinase enables phagocytosis of large particles by terminating actin assembly through Rac/Cdc42 GTPase-activating proteins. *Nat. Commun.* 6:8623. https://doi.org/10.1038/ncomms9623

Schmid, E.M., M.H. Bakalar, K. Choudhuri, J. Weichsel, H. Ann, P.L. Geissler, M.L. Dustin, and D.A. Fletcher. 2016. Size-dependent protein segregation at membrane interfaces. *Nat. Phys.* 12:704–711. https://doi.org/10.1038/nphys3678

Schneider, I. 1972. Cell lines derived from late embryonic stages of Drosophila melanogaster. *J. Embryol. Exp. Morphol.* 27:353–365.

Segawa, K., and S. Nagata. 2015. An Apoptotic 'Eat Me' Signal: Phosphatidylserine Exposure. *Trends Cell Biol.* 25:639–650. https://doi.org/10.1016/j.tcb.2015.08.003

Stinchcombe, J.C., G. Bossi, S. Booth, and G.M. Griffiths. 2001. The immunological synapse of CTL contains a secretory domain and membrane bridges. *Immunity.* 15:751–761. https://doi.org/10.1016/S1074-7613(01)00234-5

Tung, T.T., K. Nagaosa, Y. Fujita, A. Kita, H. Mori, R. Okada, S. Nonaka, and Y. Nakanishi. 2013. Phosphatidylserine recognition and induction of apoptotic cell clearance by Drosophila engulfment receptor Draper. *J. Biochem.* 153:483–491. https://doi.org/10.1093/jb/mvt014

Yamauchi, S., K. Kawauchi, and Y. Sawada. 2012. Myosin II-dependent exclusion of CD45 from the site of Fcγ receptor activation during phagocytosis. *FEBS Lett.* 586:3229–3235. https://doi.org/10.1016/j.febslet.2012.06.041

Yi, J., X.S. Wu, T. Crites, and J.A. Hammer III. 2012. Actin retrograde flow and actomyosin II arc contraction drive receptor cluster dynamics at the immunological synapse in Jurkat T cells. *Mol. Biol. Cell.* 23:834–852. https://doi.org/10.1091/mbc.e11-08-0731

Zhang, Y., J.H. Malone, S.K. Powell, V. Periwal, E. Spana, D.M. Macalpine, and B. Oliver. 2010. Expression in aneuploid Drosophila S2 cells. *PLoS Biol.* 8:e1000320. https://doi.org/10.1371/journal.pbio.1000320

Zhou, Z., E. Hartwieg, and H.R. Horvitz. 2001. CED-1 is a transmembrane receptor that mediates cell corpse engulfment in C. elegans. *Cell.* 104:43–56. https://doi.org/10.1016/S0092-8674(01)00190-8

Ziegenfuss, J.S., R. Biswas, M.A. Avery, K. Hong, A.E. Sheehan, Y.-G. Yeung, E.R. Stanley, and M.R. Freeman. 2008. Draper-dependent glial phagocytic activity is mediated by Src and Syk family kinase signalling. *Nature.* 453:935–939. https://doi.org/10.1038/nature06901

Ziegenfuss, J.S., J. Doherty, and M.R. Freeman. 2012. Distinct molecular pathways mediate glial activation and engulfment of axonal debris after axotomy. *Nat. Neurosci.* 15:979–987. https://doi.org/10.1038/nn.3135